Section 2

Data sets, diagnostic and dynamical investigations, statistical post-processing , multi-year reanalyses and associated studies

Tropospheric Lapse Rate and its Relation to Surface Temperature for warm and cold seasons from Reanalysis Data

Akperov M. G.[1]
[1]Institute of Atmospheric Physics, RAS, Moscow, Russia
aseid@ifaran.ru

Estimates of the tropospheric lapse rate γ and analysis of its relation to the surface temperature T_s in the interannual variability have been made using the global monthly mean data of the NCEP/NCAR reanalysis (1948 - 2001), in particular for warm (August) and cold (January) seasons. The tropospheric lapse rate γ for January is about 5.9 K/km in the Northern Hemisphere (NH). Over the ocean is about 6.0 and about 5.7 K/km over the continents. For August this value is about 6.3 K/km and 6.2 for ocean and 6.4 for continents. The value of γ has a maximum for the NH as a whole in August (7.0 K/km) and minimum (3.5 K/km) in January (Fig. 1).

The values of $d\gamma/dT_s$ (Fig. 2), the parameter of sensitivity of γ to the variation of T_s for the NH in the interannual variability, are found for January to be about 0.06 km^{-1} (0.060 km^{-1} for the NH as a whole, 0.055 km^{-1} over the ocean, and 0.061 km^{-1} over the continents). These values for August are about 0.038 km^{-1} (0.038 km^{-1} for the NH as a whole, 0.043 km^{-1} over the ocean, and 0.038 km^{-1} over the continents).

Positive values of $d\gamma/dT_s$ characterize a positive climatic feedback through the lapse rate and indicate a general decrease in the static stability of the troposphere during global warming (Mokhov and Akperov, 2006)(see also Mokhov 1983). Along with a general tendency of γ to increase with rising T_s, there are regional regimes with the opposite tendency, mainly over the ocean. The negative correlation of γ with T_s is found over the oceanic tropics and midlatitudes, in particular, over the oceanic belt around Antarctica (Mokhov 1993).

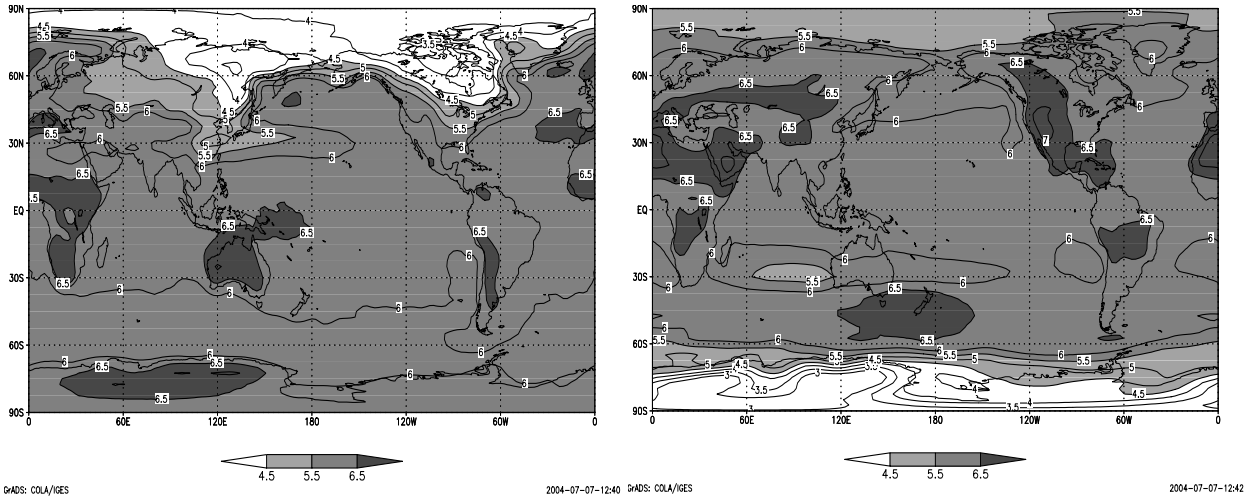

b) a)

Fig. 1. Geographical distribution of annual mean γ [K/km] for January (a) and August (b).

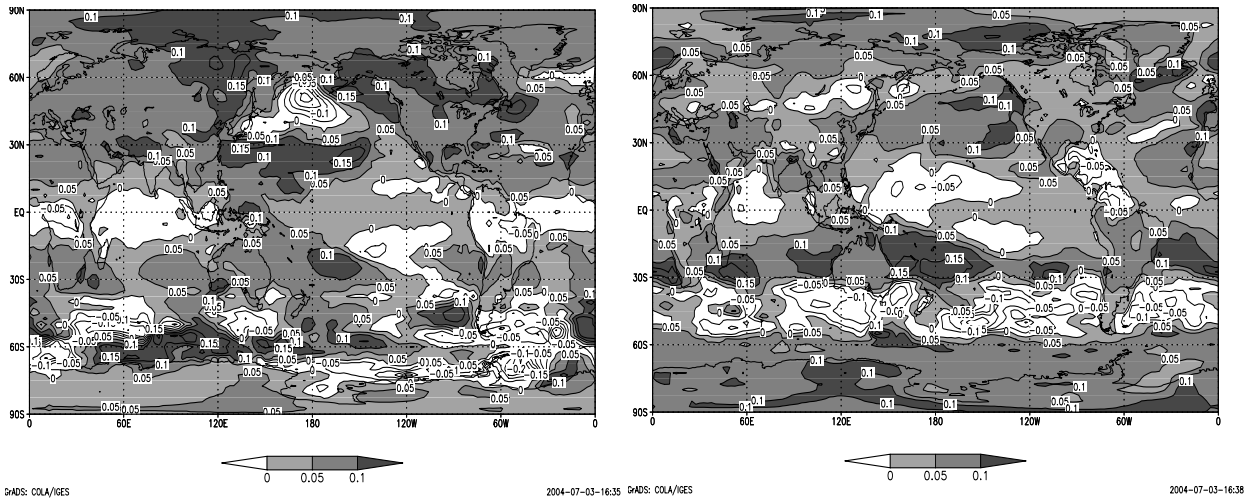

a) b)

Fig. 2. Geographical distribution of coefficients of regression of γ [K/km] to T_s [K] for January (a) and August (b).

This work was partly supported by the Russian Foundation for Basic Research, Programs of the Russian Academy of Sciences and by the Russian President Scientific Grant.

References

Mokhov I. I. and Akperov M. G. Tropospheric Lapse Rate and Its Relation to Surface Temperature from Reanalysis Data. *Izv.-Atmos. Ocean. Phys*. 2006. V. 42. №4. p. 430.

Mokhov I. I. Vertical Temperature Gradient in the Troposphere and Its Relation to the Surface Temperature from Empirical Data. *Izv.-Atmos. Ocean. Phys*. 1983. V. 19. №9. p. 913.

Mokhov I. I. Diagnostics of the Structure of a Climatic System. (Gidrometeoizdat, St. Petersburg, 1993) [in Russian].

Temperature Trends in Antarctic Atmosphere Detected by the Method Based on the Using of Hourly Observations

Oleg A. Alduchov and Irina V. Chernykh

Russian Institute of Hydrometeorological Information – Word Data Center, Obninsk, Russia,
E-mail: aoa@meteo.ru, civ@meteo.ru

Linear trends in time series of temperature anomalies at the standard isobaric levels calculated by the method based on the using of hourly observations with taking into account the possible time correlations of observations [Alduchov et al, 2006] are presented for different months, seasons and for year for eight coastal Antarctic stations

Radiosonde sounding data from CARDS [Eskridge et al, 1995] for eight stations: Bellingshausen (1970-1999 years), Halley (1966-2001 years), Novolazarevskaya (1969-2001 years), Syova (1969-2001 years), Mawson (1969-2001 years), Davis (1970-2001 years), Mirny (1969-2001 years), Casey (1969-2001 years) were used for research of climatic changes in Antarctic atmosphere.

The results are presented at the figure 1 and figure 2. The significance of the trends is not less than 50%.

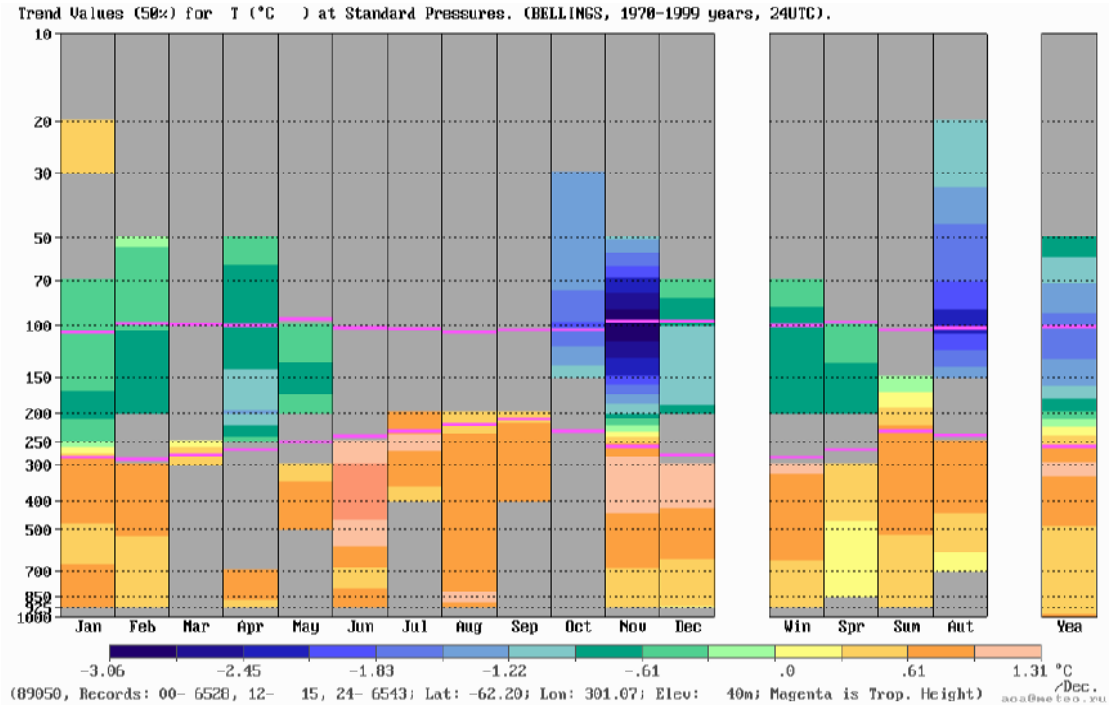

Figure 1. Linear trends for temperature anomalies (ºC) at the isobaric levels calculated on the base of hourly observations with taking into account the time correlations of observations for different months (at the right), season (in the center; winter – December, January, February) and for year (at the left). The significance of the trends is not less than 50%. The first and second tropopause is marked by pink lines. Bellingshausen. 1970-1999 years. CARDS.

Figure 1 and figure 2 show that climatic changes in Antarctic atmosphere are inhomogeneous in the time and space.

Warming in troposphere for all months (with exception October), seasons and for year is detected over Bellingshausen station only. Warming in middle and high layers of the troposphere is bigger than it is in low troposphere for all season and year.

Warming in troposphere for Australian winter (marked at the figures as “sum”) was detected for all studied stations with exception Mirny station.

Warming in troposphere for year in total was detected over Bellingshausen and very small warming was detected over Halley and in some layers of troposphere over Mawson, Davis, and Casey.

Small cooling was detected in some layers of troposphere over Novolazarevskaya and Syova stations.

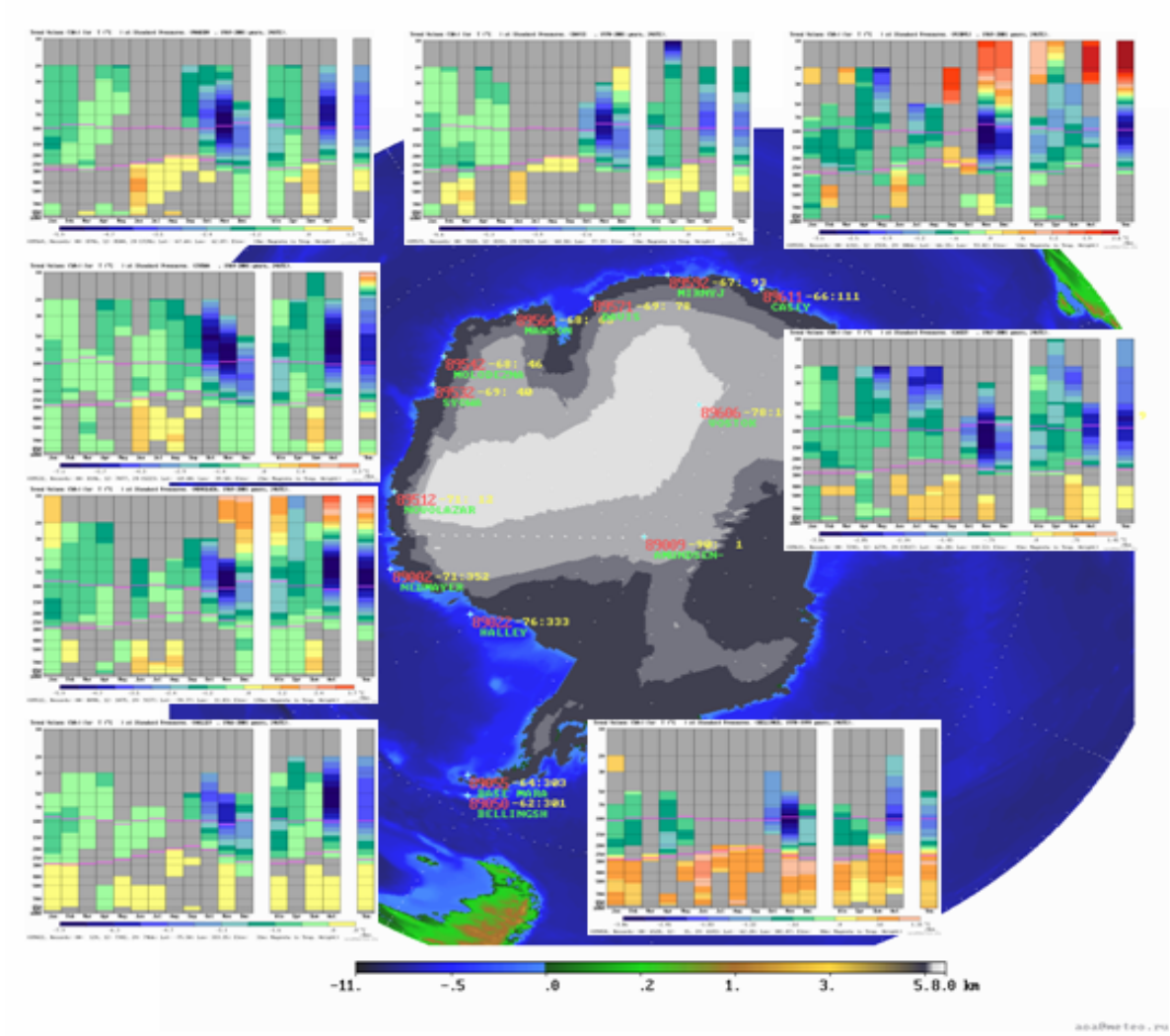

Figure 2. Corresponding linear trends for temperature anomalies (ºC) at the isobaric levels calculated on the base of hourly observations with taking into account the possible time correlations of observations for different months (at the right), season (in the center; winter – December, January, February) and for year (at the left) for Antarctic stations (from right bottom to clockwise): Bellingshausen, Halley, Novolazarevskaya, Syova, Mawson, Davis, Mirny, Casey. The significance of the trends is not less 50%. The first and second tropopause is marked by pink lines. CARDS.

Cooling in the low stratosphere was determined over all stations. But figure 2 shows the warming in high layers of stratosphere for some station (Novolazarevskaya, Syova, and Mirny). The improving of sounding system may be one of the reasons of determined cooling in stratosphere. Now sonde may up higher for more cold weather condition.

Very like that change of cloudiness is one of the reasons of Antarctic troposphere warming [Turner et al, 2006].

The results can be used for modeling of climate change, for comparison with results obtained on base other data sets.

Acknowledgment. Study was supported by subprogram “Study and research of Antarctica” of Federal program "World ocean" and Russian Basic Research Foundation (RBRF).

REFERENCES

Alduchov O.A., Lagun V. E., I.V. Chernykh, Jagovkina S.V., 2006: About climatic changes of troposphere over Antarctic peninsula. "Problemy Klimatologi Polarnej". **16**, 7-22.

Eskridge R.E., Alduchov O.A., Chernykh I.V., Zhai P., Doty S.R., Polansky A.C. A Comprehensive Aerological Reference Data Set (CARDS): Rough and systematic errors. - Bull. Amer. Meteor. Soc., 1995, v. 76, p. 1959-1775.

Turner J., Lachlan–Cope T.A., Colwell S., Marshall G. J., Connolley W.M. Significant warming of the Antarctic winter troposphere. – Science, 2006, v. 311, p. 1914-1917.

Cloudiness anomalies and El Nino effects

A.V. Chernokulsky
A.M. Obukhov Institute of Atmospheric Physics RAS, Moscow, Russia
chern_av@ifaran.ru

Effects of El Nino on cloudiness from ISCCP data (Rossow and Duenas, 2004) in periods 1983-2005 years are estimated. Most significant differences in cloudiness are noted over tropical and equatorial latitudes in the eastern part of the Pacific Ocean in December-January-February (Fig. 1) (Mokhov and Chernokulsky 2003; Chernokulsky and Mokhov, 2006). Positive anomaly in this region reaches 0.4 in El Nino years (years with the largest positive anomalies of Nino 3 SST (5°N-5°S 150°W-120°W) (Rayner et al, 2003)). At the same time about 2/3 of these changes are related to the changes in cirrus and cirrostratus clouds (Fig. 2) contributing to the greenhouse effect. The mutual dynamics of temperature and cloudiness in this region should lead to the positive feedback.

There are negative cloudiness anomalies in the equatorial latitudes in the western part of the Pacific Ocean and in the eastern part of Indian Ocean. Cloud amount decreases in El Nino years by 0.1-0.2 and depends basically on changes in cirrus and cirrostratus clouds.

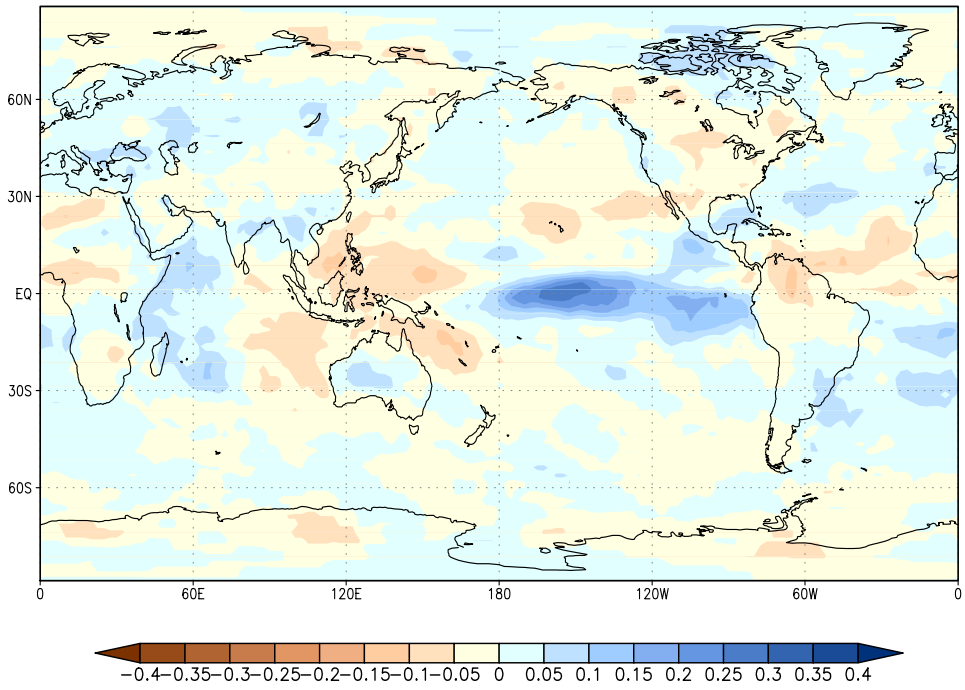

Fig. 1 Difference for total cloudiness in December-January-February between 5-year-means for years with the largest positive anomalies of the Nino 3 SST (1986-87, 1991-92, 1994-95, 1997-98, 2002-03) and neutral years (1989-90, 1990-91, 1992-93, 1993-4, 2004-05).

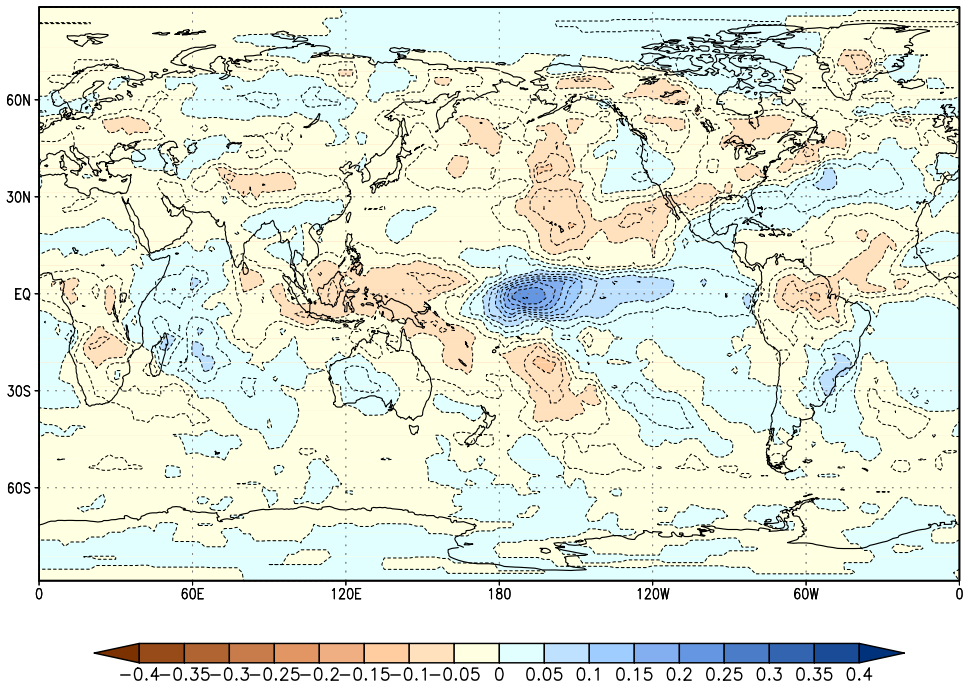

Fig. 2 Difference for cirrus and cirrostratus clouds in December-January-February between 5-year-means for years with the largest positive anomalies of the Nino 3 SST (1986-87, 1991-92, 1994-95, 1997-98, 2002-03) and neutral years (1989-90, 1990-91, 1992-93, 1993-4, 2004-05).

This work was partly supported by the Russian Foundation for Basic Research, Programs of the Russian Academy of Sciences and by the Russian President Scientific Grant.

References

Chernokulsky A.V., Mokhov I.I. Global and Regional Cloudiness Changes by Satellite Data: Relationship with Temperature and El Nino Effects // Research Activities in Atmospheric and Oceanic Modelling. J. Cote (ed.). 2006. WMO/TD-No.1347, P.02.09-02.10

Mokhov I.I., Chernokulsky A.V. Global cloudiness: Tendencies of Change from ISCCP data, // Research Activities in Atmospheric and Oceanic Modelling. J. Cote (ed.). J. Cote (ed.). 2003. WMO/TD-No.1161. P.02.07-02.08.

Rossow, W.B., and E. Duenas, 2004: The International Satellite Cloud Climatology Project(ISCCP) web site: An online resource for research.// *Bull. Amer. Meteorol. Soc.* ***85***, 167-172.

Rayner N. A., D. E. Parker, E. B. Horton, C. K. Folland, L. V. Alexander, D. P. Rowell, E. C. Kent, A. Kaplan, Global analyses of sea surface temperature, sea ice, and night marine air temperature since the late nineteenth century. // *J. Geophys. Res*., 108 (D14), 4407, doi:10.1029/2002JD002670, 2003.

About Accuracy of High Cloud Amount Detecting from Radiosonde Sounding

Irina V. Chernykh

All Russian Institute of Hydrometeorological Information – Word Data Center, Obninsk, Russia,
E-mail: civ@meteo.ru

Research of thin high cloud layers is especially important due problem of its true detection by satellite and surface observations, from radiosonde sounding data. Difficulties in thin clouds detection is one of the reasons of different cloudiness climatologies obtained on base different platform of observations (Poore et al., 1995; Rossow and Dueñas, 2004; Chernykh, 2001; Chernykh and Aldukhov, 2004).

According previous study (Chernykh, 2001), surface observations indicate that frequency of one-four thin cloud layers comes for some stations to 35% from all observations. But for high clouds, as it follows from Table 1 and Table 2, surface observations indicate that frequency of thin cloud layers comes to 86% from all high cloud observations with one reported cloud layer. Frequency of thin transparent high cloud layers foots up to 26% from all thin cloud layers (see No in Table 2). But big lag error of humidity sensor is the reason for a lack of methods, based on using of the measured values of humidity (Chernykh, Eskridge, 1996; Chernykh, Alduchov, 2002; Chernykh, Aldukhov, 2004).

Main goals of this study are: to evaluate the CE method (Chernykh and Eskridge, 1996; Chernykh and Aldukhov, 2004) ability of cloud layers prediction from temperature and humidity profiles for thick and thin high cloud layers for regions with different climatic conditions; to estimate the accuracy in predicting of cloud amount and the dependence of the results on the transparency of cloud layers.

Twice-daily radiosonde sounding data and surface-based cloud observations for 1975-80 period (NCDC, 1991) for eight stations, placed in regions with different climatic conditions are using for this research (for more details see Chernykh, 2001). The observations with one reported cloud layer were included in this study. Below, opaque part exceeds 50% of the cloud amount (the transparent part is less than 50% of the cloud amount) for thick cloud layers and for thin cloud layers vice versa (NCDC, 1991). In total 3843 cases were used for analysis: 537 cases of thick and 3306 cases for thin high cloud layers (see Table 1 and Table 2).

Statistics for observations with one observed layer that is thick or thin high cloud layer: the percent of correctly diagnosed cloud level reports; the percent of correctly diagnosed cloud level and cloud cover; the percents of correctly diagnosed cloud level and overestimated/underestimated cloud amount; average cloud amount (% of the sky) calculated from surface observations presented in Table 1 and Table 2. In addition, to estimate the dependence of the results on the transparency of cloud layers the same statistics were calculated in assumption that cloud cover equal to opaque. This results are presented in Table 3.

TABLE 1. Statistics for observations with one observed layer that is thick high cloud layer. P_l is the percent of correctly diagnosed cloud level reports; P_c is the percent of correctly diagnosed cloud level and cloud cover. The difference, d, between observed, A_o, and the predicted cloud amount interval (A_p1, A_p2) is defined as $d = A_o - A_p2$ if $A_p2 < A_o$, and $d = A_p1 - A_o$ if $A_o < A_p1$. P_u1 and P_u2 are the percents of correctly diagnosed cloud level and underestimated cloud amount: $A_p2 < A_o$ and $0 < d \leq 20\%$ (for P_u1) or $d > 20\%$ (for P_u2). P_o1 and P_o2 are the percents of correctly diagnosed cloud level and overestimated cloud amount $A_o \leq A_p1$ and $0 < d \leq 20\%$ (for P_o1) or $d > 20\%$ (for P_o2). A_a is the average cloud amount (%) calculated from surface observations and N is the number of observations with one reported cloud layer. 1975 - 1980 years.

Station	P_l	P_c	P_u1	P_u2	P_o1	P_o2	A_a	N
Point Barrow	71.4	35.7	0	0	14.3	21.4	89	14
Spokane	90.9	42.4	3.0	33.4	12.1	0.0.	90	33
Albany	96.2	36.5	1.9	48.1	9.6	0.0	89	52
Medford	96.5	52.6	1.8	35.1	7.0	0.0	93	57
Ele	87.9	24.2	0.0	48.5	3.0	12.1	94	66
Cape Hatteras	89.8	51.6	0.0	30.5	7.8	0.0	94	128
Amarillo	96.7	53.8	0.0	38.5	4.4	0.0	93	91
Brownsville	96.9	61.5	1.0	21.8	12.5	0.0	86	96

TABLE 2 is the same as TABLE 1 but for one observed layer that is thin high layer. No is the number of observations with transparent thin high cloud layer.

Station	P_l	P_c	P_u1	P_u2	P_o1	P_o2	A_a	N0	N
Point Barrow	74.9	29.1	9.1	6.9	5.2	24.6	42	66	175
Spokane	94.6	32.1	14.8	23.6	7.1	17.0	47	99	352
Albany	95.1	34.9	13.6	22.1	7.5	17.0	46	63	384
Medford	95.7	34.1	12.0	26.4	7.0	16.1	51	111	299
Ele	91.9	30.9	12.5	24.1	4.4	20.0	49	141	456
Cape Hatteras	93.8	31.6	10.7	24.1	6.2	21.2	53	114	661
Amarillo	97.5	34.8	13.9	24.5	7.2	17.0	46	202	652
Midway	82.8	17.3	13.8	24.1	3.5	24.1	50	6	29
Brownsville	96.3	28.2	12.4	15.4	11.3	29.2	42	54	298

TABLE 3 is the same as TABLE 1 but for one observed layer that is thin high layer with opaque more than zero. P_c is the percent of correctly diagnosed cloud level and opaque of cloud layer. A_a is the average cloud amount (%) for opaque of cloud layer, calculated from surface observations.

Station	P_l	P_c	P_u1	P_u2	P_o1	P_o2	A_a	N
Point Barrow	70.6	21.1	4.6	0.0	4.6	40.4	20	109
Spokane	94.5	40.7	13.4	1.2	2.8	36.4	22	253
Albany	94.7	44.5	13.7	1.2	3.4	31.8	22	321
Medford	95.2	40.4	15.4	1.1	4.3	34.0	21	188
Ele	90.5	41.9	11.1	0.6	1.9	34.9	20	315
Cape Hatteras	93.2	34.7	12.6	2.4	4.0	39.5	22	547
Amarillo	97.1	44.2	12.7	0.7	2.9	36.7	21	450
Midway	87.0	34.8	13.0	0.0	0.0	39.1	22	23
Brownsville	96.3	34.4	10.7	1.2	4.9	45.1	21	244

Conclusion: Results, presented in Table1 – Table 3 for high clouds, have shown that frequency of correctly diagnosed cloud level and cloud cover P_c depends from transparency of cloud layer. The more opaque part of cloud layers the more frequency of correctly diagnosed cloud level and cloud cover P_c. CE-method gives a possibility to enough realistic reflect thin high cloud layers forming: predicted cloud amount is greater than opaque, but less than total cloud cover, which includes transparent part of cloud layers.

Results can be used for modeling of atmospheric circulation and cloud modeling, for comparison with results obtained on base satellites.

Acknowledgment. Study was partly supported by Russian Basic Research Foundation (RBRF), project № 04-05-64681.

REFERENCES

Chernykh I. V. ,2001: Reconstructed Clouds Layers Thickness for Different Sky Conditions. Research Activities in Atmospheric and Oceanic Modelling. WMO. No. 31. Geneva. 2.8-2.9 pp.

Chernykh I.V., O.A. Alduchov, 2002: Detection of Cloudiness from Temperature and Humidity Profiles for Different Resolution of Radiosonde Sounding by Various Methods. Research Activities in Atmospheric and Oceanic Modelling. WMO. No. 32 Geneva. 2.5-2.6.

Chernykh I.V. and O.A. Aldukhov, 2004: Vertical Distribution of Cloud Layers from Cloud Radiosounding Data. Izvestiya, Atmospheric and Oceanic Physics. Vol. 40, No 1, 2-004, pp. 41-53.

Chernykh I.V. and R.E. Eskridge, 1996: Determination of cloud amount and level from radiosonde soundings. *J.Appl. Meteorol,* ***35****,* 1362-1369 pp.

NCDC, 1991: TD-3280 Surface Airways Hourly. Internal Report of the National Climate Data Center, 40pp.

Poore K.D., J. Wang, W.B. Rossow, 1995: Cloud Layer Thickness from a Combination of Surface and Upper-Air Observations. *J. Climate*, 8, pp. 550-568.

Rossow W. B. and E. N. Dueñas, 2004: The International Satellite Cloud Climatology Project (ISCCP) Web Site: An Online Resource for Research Bulletin of the American Meteorological Society: Vol. 85, No. 2, pp. 167–172.

Trends in Low Cloud Boundary for Antarctic Region

Irina V. Chernykh and Oleg Alduchov

Russian Institute of Hydrometeorological Information – Word Data Center, Obninsk, Russia,
E-mail: civ@meteo.ru, aoa@meteo.ru

It have been detected for Globe for the period 1964-1998 years that low boundary (ceiling) means for cloud layers (CL) with cloud amount 0-100% of the sky (CA_0-100) in atmospheric layer 0-10 km are decreasing for central month of the season (January, April, July, October) separately and in total with decadal changes means in m decade^{-1}: -35; -49; -51; -41 and -43 correspondently [Chernykh et al, 2001]. The significance of the trends is not less than 95%. The mean values and trends of low boundary (LB) for CL with CA_0-100 are presented in this paper for Antarctic region for different atmospheric layers in detail: for different months, seasons and for year. In reality, LB for CL with CA_0-100 specifies the beginning of temperature-humidity layering of atmosphere. It should be noted, that LB value, detected by different method, can be some different due different accuracy of determination method [Chernykh and Alduchov 2004; Naud et al, 2003].

The investigation was made on base of dataset contained time series of cloud boundaries and cloud amount for cloud layers, created on the base of radiosonde sounding data CARDS [Eskridge et al, 1995] and CE-method for cloud amount and boundaries reconstruction [Chernykh and Eskridge, 1996; Chernykh and Alduchov 2004] for Antarctic stations. Seven coastal stations (Bellingshausen (1970-1999), Halley (1966-2001), Novolazarevskaya (1969-2001), Mawson (1969-2001), Davis (1970-2001), Mirny (1969-2001), Casey (1969-2001)) were selected for research.

Linear trends in LB of CL with CA_0-100 were calculated by the method based on the using of time series with taking into account the possible time correlations of observations [Alduchov et al, 2006].

Multiannual averages of LB and decadal changes for year of LB of CL with CA_0-100 in different atmospheric layers are presented in Table1.

Table 1. Multiannual averages (m) of LB (in meters) and decadal changes (Δ) of LB (in meters decade^{-1}) of CL with CA_0-100 in different atmospheric layers. The significance of the trends is not less than 50%. Trend value with significance not less than 95% marked *.

Station	Atmospheric layer							
	0-2 km		2-6 km		6-10 km		0-10 km	
	m	Δ	m	Δ	m	Δ	m	Δ
Bellingshausen	488	-35*	2794	-	6850	-	723	-66*
Halley	590	18	2811	-76*	6786	-44*	1029	-184*
Novolazarevskaya	701	12	2560	-23*	6812	-60*	852	-41*
Mawson	606	-35*	2551	-79*	6698	-181*	652	-28
Davis	527	-24*	2612	-126*	6717	-196*	590	-
Mirny	625	54*	2766	-48*	6855	-70*	864	-30
Casey	496	20*	2590	-106*	6668	-173*	576	-61*

Mean values for LB of CL with CA_0-100 in atmospheric layers 0-2 km, 2-6 km, 6-10 km, 0-6 km, 2-10 km, 0-10 km over surface level are presented at fig.1a for different months, seasons and for year. Figure 1a shows specific properties (mean values and its annual variations) of LB of CL with CA_0-100 in different atmospheric layers for the stations. Figure 1b demonstrates that climatic changes of the LB of temperature-humidity layering in atmosphere over Antarctica are inhomogeneous in the time and space. The significance of the trends is not less than 50%.

Acknowledgment. Study was partly supported by subprogram “Study and research of Antarctica” of Federal program "World ocean" and Russian Basic Research Foundation (RBRF).

REFERENCES

Alduchov O.A. , Lagun V. E., I.V. Chernykh, *Jagovkina S.V.,* 2006: About climatic changes of troposphere over Antarctic peninsula. "Problemy Klimatologi Polarnej". **16**, 7-22.

Chernykh I.V., O.A. Alduchov, R. E. Eskridge, 2001: Trends in low and high cloud boundaries and Errors in height determination of cloud boundaries. Bull. of Amer. Met. Society., **82,** 1941–1947.

Chernykh I.V. and O.A. Aldukhov, 2004: Vertical Distribution of Cloud Layers from Cloud Radiosounding Data. Izvestiya, Atmospheric and Oceanic Physics. **40**, 1, 2004, pp. 41-53.

Chernykh I.V. and R.E. Eskridge, 1996: Determination of cloud amount and level from radiosonde soundings. *J.Appl. Meteorol,* ***35****,* 1362-1369 pp.

Naud C.M., Muller J.P., E.E. Clothiaux, 2003: Comparison between active sensor and radiosonde cloud boundaries aver the ARM Southern Great Plains site. *J. Geophysical research,* **108**, D4, 3-1 – 3-12.

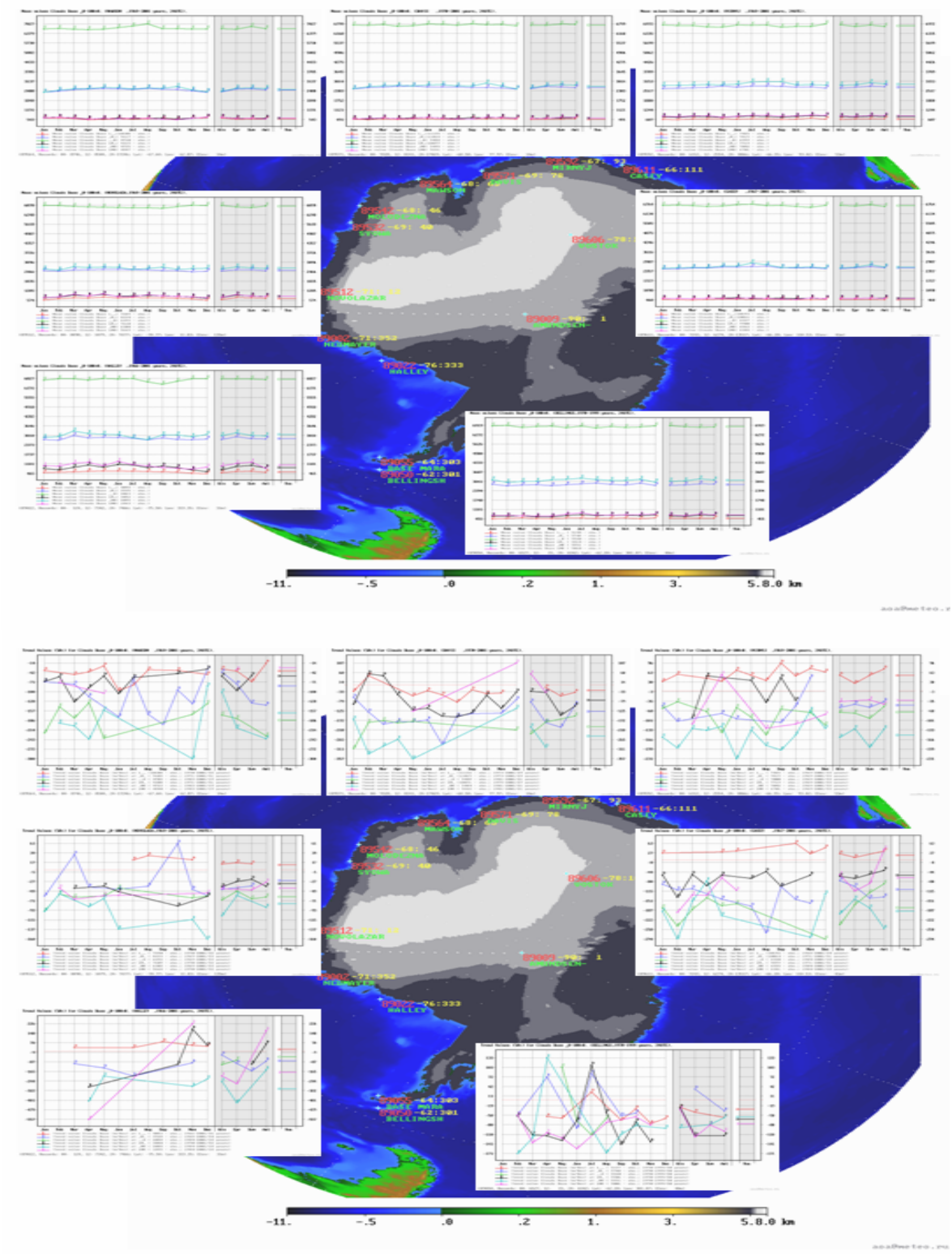

Figure 1. (a) Mean values for low boundary of cloud layers with cloud amount 0-100% for different months (at the left), seasons (in the center; winter – December, January, February) and for year (at the right) in different atmospheric layers: 0-2 km - (A, red lines), 2-6 km - (B, navy lines), 6-10 km - (C, green lines), 0-6 km – (D, black lines), 2-10 km – (E, blue lines), 0-10 km – (I, pink lines). (b) Corresponding trends. The significance of the trends is not less than 50%. Antarctic stations (from bottom to clockwise): Bellingshausen, Halley, Novolazarevskaya, Mawson, Davis, Mirny, Casey.

Trends in Low Boundary of Cloud Layers with Cloud Amount 80-100% of the Sky for Antarctic Region

Irina V. Chernykh and Oleg A. Alduchov

Russian Institute of Hydrometeorological Information – Word Data Center, Obninsk, Russia,
E-mail: civ@meteo.ru, aoa@meteo.ru

It have been shown for Globe for the period 1964-1998 years that low boundary (ceiling) means for cloud layers (CL) with cloud amount 80-100% of the sky (CA80) in atmospheric layer 0-10 km are decreasing for central month of the season (January, April, July, October) separately and in total with decadal changes of -27 m/decade, -27 m/decade, -19 m/decade, -25 m/decade and -24 m/decade correspondently [Chernykh and Alduchov, 2000; Chernykh et al, 2001]. The significance of the trends is not less than 95%. The estimations of low boundary (LB) means for CL with CA80 and trends in LB are presented in this paper for Antarctic region more particularly: for different months, seasons and for year for different atmospheric layers.

Dataset contained time series of cloud boundaries and cloud amount for CL, created on base radiosonde sounding data CARDS and CE-method for cloud amount and boundaries reconstruction [Chernykh and Eskridge, 1996; Chernykh and Alduchov 2004] for Antarctic region were used for the investigation. Seven coastal Antarctic stations: Bellingshausen (1970-1999 years), Halley (1966-2001 years), Novolazarevskaya (1969-2001 years), Mawson (1969-2001 years), Davis (1970-2001 years), Mirny (1969-2001 years), Casey (1969-2001 years) were selected for research.

Linear trends were calculated by the method based on the using of observations with taking into account the possible time correlations of observations [Alduchov et al, 2006].

Mean values and trends for LB of CL with CA80 for the atmospheric layers 0-2 km, 2-6 km, 6-10 km, 0-6 km, 2-10 km, 0-10 km over surface level are presented at figure 1. The significance of the trends is not less than 50%.

For example (figure 1a) multiannual averages for LB of CL with CA80 in the atmospheric layer 0-2 km are 0.5 km for Bellingshausen, 0.6 km - for Halley, 1.2 km – for Novolazarevskaya, 1.2 km - for Mawson, 0.9 km - for Davis, 0.9 km – for Mirny and 0.7 km for Casey. In atmospheric layer 0-10 km they are about 1.8 km for Bellingshausen, 2 km - for Halley, 4.1 km – for Novolazarevskaya, 2.5 km - for Mawson, 2 km - for Davis, 3.4 km – for Mirny and 1.7 km for Casey.

Figure 1b demonstrates that climatic changes of LB for overcast condition of the sky in Antarctic atmosphere are inhomogeneous in the time and space.

Decreasing of LB in atmospheric layer 0-10 km for year was detected for stations: Bellingshausen, Novolazarevskaya, Mawson and Davis with decadal changes in km decade^{-1}: 0.2; 0.3; 0.1 and 0.3.

Small decreasing of LB in atmospheric layer 0-2 km for year was detected for stations: Bellingshausen, Mawson and Davis with decadal changes in m decade^{-1} 30; 13; 13 correspondently.

Small increasing of the LB in atmospheric layer 0-2 km for year was detected for stations: Halley and Mirny with decadal changes in m decade^{-1}: 20 and 60 correspondently.

Increasing of cloud amount over the stations can lead to decreasing of LB of CL with CA80 and vice versa decreasing of cloud amount over the stations can lead to increasing of LB of CL with CA80. Changes in the frequencies of different cloud types can lead to detected LB changes too.

The results can be used for comparison with results obtained on base surface and satellites observations, in aviation needs.

Acknowledgment. Study was supported by subprogram “Study and research of Antarctica” of Federal program "World ocean" and Russian Basic Research Foundation (RBRF).

REFERENCES

Alduchov O.A. , Lagun V. E., I.V. Chernykh, *Jagovkina S.V.,* 2006: About climatic changes of troposphere over Antarctic peninsula. "Problemy Klimatologi Polarnej". **16**, 7-22.

Chernykh I.V. and O.A. Alduchov, 2000: Trends of Some Parameters of the Cloudy Sky Reconstructed from CARDS of 1964-1998. Proceedings of 24 Annual Climate Diagnostics and Prediction Workshop. Arizona. November 5-9, 1999. 187-190 pp.

Chernykh I.V. and O.A. Aldukhov, 2004: Vertical Distribution of Cloud Layers from Cloud Radiosounding Data. Izvestiya, Atmospheric and Oceanic Physics. Vol. 40, No 1, 2-004, pp. 41-53.

Chernykh I.V., O.A. Alduchov, R. E. Eskridge, 2001: Trends in low and high cloud boundaries and Errors in height determination of cloud boundaries. Bull. of Amer. Met. Society., **82,** 1941–1947.

Chernykh I.V. and R.E. Eskridge, 1996: Determination of cloud amount and level from radiosonde soundings. *J.Appl. Meteorol,* ***35,*** 1362-1369 pp.

Eskridge, R.E., O.A. Alduchov, I.V. Chernykh, P. Zhai, A.C. Polansky, and S.R. Doty, 1995: A comprehensive aerological reference dataset (CARDS): rough and systematic errors. Bull. Amer. Meteor. Soc., 76, 1759-1775.

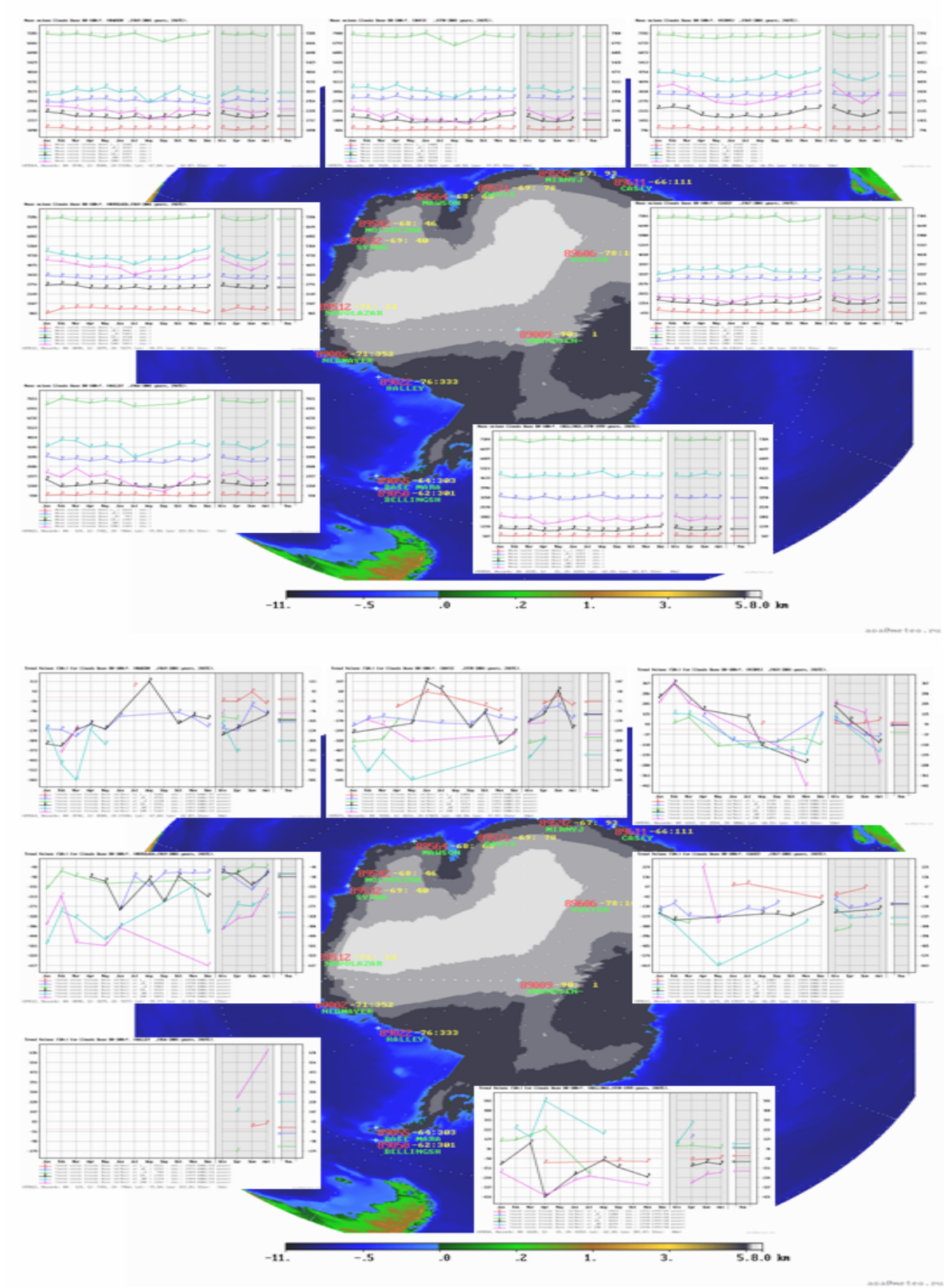

Figure 1. (a) Mean values for low boundary of cloud layers with cloud amount 80-100% of the sky for different months (at the left), seasons (in the center; winter – December, January, February) and for year (at the right) in different atmospheric layers: 0-2 km - (A, red lines), 2-6 km - (B, navy lines), 6-10 km - (C, green lines), 0-6 km – (D, black lines), 2-10 km – (E, blue lines), 0-10 km – (I, pink lines). (b) Corresponding trends. The significance of the trends is not less than 50%. Antarctic stations (from bottom to clockwise): Bellingshausen, Halley, Novolazarevskaya, Mawson, Davis, Mirny, Casey.

Hindcasts of historic storms with GME, COSMO-LMQ, and COSMO-LMK

Helmut P. Frank, Detlev Majewski
Deutscher Wetterdienst, Kaiserleistr. 42, D-63067 Offenbach/Main, Germany

Introduction

NLWKN (`www.nlwkn.de`), the Coastal Research Station of Lower Saxony Water Management, Coastal Defence and Nature Conservation Agency, contracted Deutscher Wetterdienst (German Weather Service, DWD) to provide high resolution wind fields during strong storms for flood predictions near the Ems river estuary in northwestern Germany. NLWKN chose 22 storms from the famous Hamburg Storm in February 1962 to a storm in October 2002.
DWD produced wind fields during these storms using its model chain GME, COSMO-LMQ, and COSMO-LMK starting from ERA-40 reanalysis data (Frank and Majewski, 2006). The wind fields will be used by NLWKN for coastal protection studies.
A series of 18 hour forecasts starting from 00 and 12 UTC analysis data was used to obtain high resolution hourly wind fields along the German North sea coast with a grid spacing as small as 2.8 km. To allow for an adaptation of the models to the initial fields only forecasts from 6 to 18 hours are provided to NLWKN. The 6 and 18 hour forecasts for the same verification time are averaged.

Model description and setup

The global model GME is a hydrostatic weather prediction model (Majewski et al., 2002). It operates on the icosahedral-hexagonal grid. The model has a mesh size of approximately 40 km and 40 layers up to 10 hPa with a hybrid vertical coordinate system. For these hindcasts the initial state was interpolated from the ECMWF ERA-40 reanalysis (Uppala and et al., 2005) to the GME grid.
The ERA-40 reanalysis was done with ECMWF's IFS model using a spherical harmonics representation T_L159 and a reduced Gaussian grid corresponding approximately to a mesh size of 125 km
The COSMO model (Steppeler et al., 2003, `www.cosmo-model.org`) is a non-hydrostatic limited-area atmospheric prediction model operating on the meso-β and meso-γ scale. It uses a regular C-grid in rotated geographical coordinates. It is used here in two different setups.

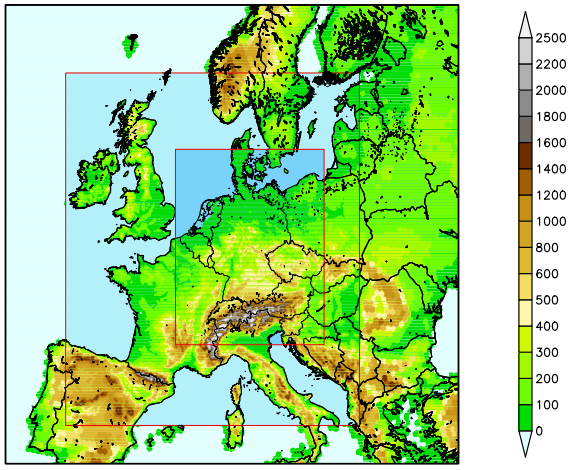

Figure 1: Model orography and nesting of LMQ in GME and LMK in LMQ.

The COSMO-LMQ model has a mesh size of 7 km (0.0625°). A leap-frog scheme with a time step of 40 s is used for time integration. Deep and shallow convection are parameterized using the mass flux approach of Tiedtke (1989). The model domain consists of 333×333 grid points.
The COSMO-LMK model has a mesh size of only 2.8 km (0.025°). It is assumed that deep convection can be explicitly resolved by the model. Only shallow convection is parameterized through moisture convergence in the planetary boundary layer similar. For time stepping a Runge-Kutta scheme of 3rd order with time step 30 s is used.
The initial state for LMQ is interpolated from the GME, and the initial state for LMK from LMQ. Lateral boundary values are updated hourly from GME, and LMQ, respectively. The nesting of LMK in LMQ and of LMQ in GME is shown in Figure 1.

The storm on 3 December 1999

As an example we present a few results for the storm on 3 December 1999. This was the strongest observed storm in Denmark. Sea level pressure dropped to 952 hPa.

The observed sea level pressure and 10 m wind on the island Norderney is compared with the different model hindcasts in Figure 2. Breaks in the curves show the difference from one 18 h forecast to the 6 h forecast of the following run. The small scale COSMO models LMQ and LMK show lower the minimum pressure than the global models. GME, LMQ, and LMK calculate similar wind maxima. However, the maximum occurs one or two hours too early in the model runs. The ERA-40 forecast gives much weaker 10 m winds because the pressure gradient is weaker. In addition, the sea surface roughness, z_0, is greater – over 5 cm compared to approximately 2 mm for the DWD models.

The strongest winds occur in the cold sector south and southwest of the center (Figure 3). Naturally, LMK shows much more details than the other models. Also, it is the only model to resolve the east Friesian islands off the German and Dutch North Sea coast.

The ERA-40 resolution is too coarse to capture the small cyclone. Buizza and Hollingsworth (Winter 2000/01) showed that a high-resolution ensemble prediction system (T_L255) predicted this storm much better than the ensemble prediction system with then T_L159 which is the same resolution as the ERA-40 reanalysis.

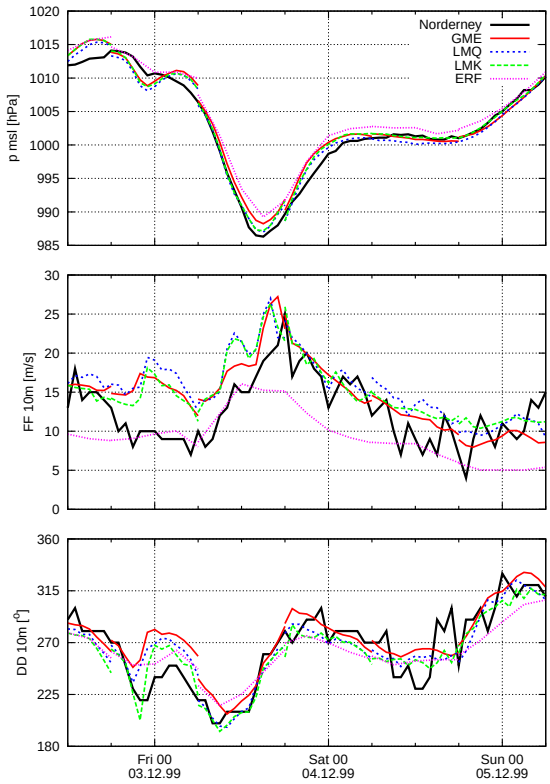

Figure 2: Time series of sea level pressure, wind speed FF, and wind direction DD observed at DWD station Norderney and predicted by the models. ERF is the ERA-40 forecast data every 3 hours.

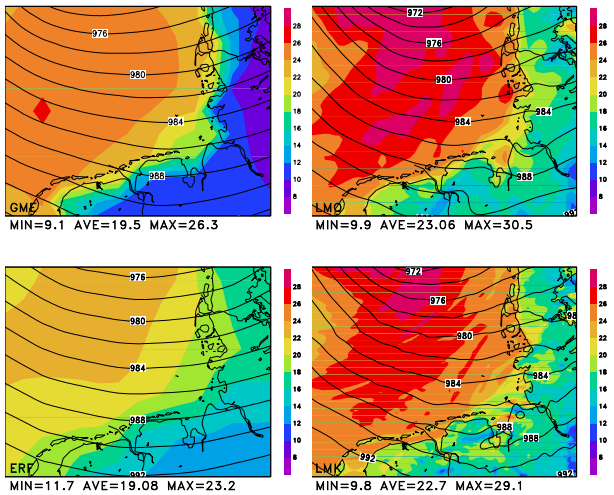

Figure 3: Mean wind speed at 10 m in $m\,s^{-1}$ at 15 UTC on 1999-12-03 simulated by GME (top left), LMQ (top right), LMK (bottom right), and the ERA-40 forecast (bottom left) initialised at 15 UTC on 1999-12-03.

Acknowledgments

The calculations and a first analysis were made by Nils Kaiser and Katharina Klein from the University of Bonn, and Kai Sven Radtke from the University of Leipzig.

References

Buizza, R. and A. Hollingsworth, Winter 2000/01: *ECMWF Newsletter*, **89**, 2–12.

Frank, H. P. and D. Majewski, 2006: *ECMWF Newsletter*, **109**, 16–21.

Majewski, D., D. Liermann, P. Prohl, B. Ritter, M. Buchhold, T. Hanisch, G. Paul, and W. Wergen, 2002: *Mon. Wea. Rev.*, **130**, 319–338.

Steppeler, J., G. Doms, U. Schättler, H. W. Bitzer, A. Gassmann, U. Damrath, and G. Gregoric, 2003: *Meteorol. Atmos. Phys.*, **82**, 75–96.

Tiedtke, M., 1989: *Mon. Wea. Rev.*, **117**, 1779–1800.

Uppala, S. M. and et al., 2005: *Q. J. R. Meteorol. Soc.*, **131**, 2961–3012.

Variability in the Teleconnection Between ENSO and West Antarctic Climate

Scott Gregory, David Noone, and David Schneider

Department of Atmospheric and Oceanic Sciences and Cooperative Institute for Research in the Environmental Sciences, University of Colorado, Boulder, Colorado, USA

(email: scott.gregory@colorado.edu)

The atmospheric coupling between ENSO and Antarctica is not well characterized, though it has been the subject of considerable study (Turner 2004). Importantly, climate models do not reliably reproduce the differences in ENSO response at high latitudes, and, as such, without more detailed understanding of the linkage between the tropics and high latitudes, estimates of high latitude climate from climate models could be misleading. The primary reason for the poorly defined teleconnection is the fact that no two ENSOs are alike; geographically similar events can have seasonal differences and seasonally similar events will differ geographically. These are the rudimentary differences in the tropics from one event to the next but there is also high latitude decadal variability in ENSO that is highlighted by Zhang et al (1997) who exposed what is now recognized as the Pacific Decadal Oscillation (PDO). The PDO index indicates the magnitude of the leading mode of variability of north Pacific SST, north of 20 degrees N. In the southern hemisphere, there is not a similar proxy yet established for an analogous decadal oscillation. Though such a decadal oscillation hasn't been specifically identified in the south, the ITASE 2001-5 ice core (Steig, et al 2005), extracted from Antarctica near the Pacific, isotope signal correlated with the Southern Oscillation Index (SOI- an ENSO proxy) shows decadal variability that appears representative of a South Pacific decadal oscillation, perhaps coupled to the PDO. In the current study, 20th century sea level pressures from the Hadley Center are analyzed to establish their correlation with ENSO and the $\delta^{18}O$ isotope in the ITASE 2001-5 ice core in three distinct quasi-decadal epochs of high ENSO activity. These correlations are established with the intent of understanding climate variability from Antarctic proxy records with a GCM with stable water isotope fractionation through simulating tropical and perhaps global atmospheric teleconnection to Antarctica on ENSO and longer timescales.

Figure 1 shows, for three approximately 20 year epochs, the correlation between the isotope records from an ice core in West Antarctica and the SLP data. The ENSO signals were the subject of the initial investigations into the ITASE 2001-5 ice core signals. The core is dated at monthly intervals for approximately the past 200 years and the SOI dated at monthly intervals is available from the 1870's to present, allowing us to focus on the Semptember-November statistics when ENSO events are typically mature and the influence of ENSO on Antarctic is strongest (Fogt and Bromwich, 2006). Analysis of the ice core record with a 20 year moving correlation window identified an apparent oscillation in the correlation in the 20th century where at the beginning of the century there is a positive correlation, in the middle of the century it is negative, and at the end of the century it returns to positive. Since the SOI is positive for the La Niña conditions, this observation suggested that at the beginning and end of the centuries the anomalously high $\delta^{18}O$ signals were attributable, at least in part, to La Niña, while in the middle of the century they were attributable, at least in part, to El Niño. This result is affirmed by correlating the $\delta^{18}O$ signal with spatial patterns of SST and SLP which show circulation anomalies around Antarctica in phase with expected teleconnections. Wavelet analysis of the $\delta^{18}O$ and SOI showed that there were epochs at the beginning, middle, and end of the century that ENSO was especially active, shown by higher amplitudes in the 3-6 year periods of SOI spectrum and during these times there are higher amplitudes of the 3-6 year periods in the $\delta^{18}O$ spectrum. For the purpose of isolating the variance associated with ENSO, the data were separated both into the three epochs (1902-1920, Figures 1a and d; 1938-1960, Figures 1b and e; 1970-1995, Figures 1c and f) of high ENSO activity and into variability associated with ENSO frequencies (3-6 years) and lower frequencies (greater 6 years). The high frequency correlations show an ENSO related (Turner 2004) pressure anomaly of the western Antarctic Peninsula while the low frequencies show, among other features, a trend toward lower pressure at the south pole that may be associated with ozone loss (Thompson and Solomon, 2002).

This work establishes the patterns, and changes in patterns, that link ENSO to the Antarctic, and which should be reproduced in GCMs if models are to adequately account for tropical variability on the

high latitudes. The SLP-$\delta^{18}O$ correlation maps of the ENSO band of 3-6 years will be the primary target for the ENSO teleconnection to Antarctica in ongoing GCM experiments, while the lower frequency variability will be targeted for simulating features such as the decadal variability and secular trends that imply changing climate.

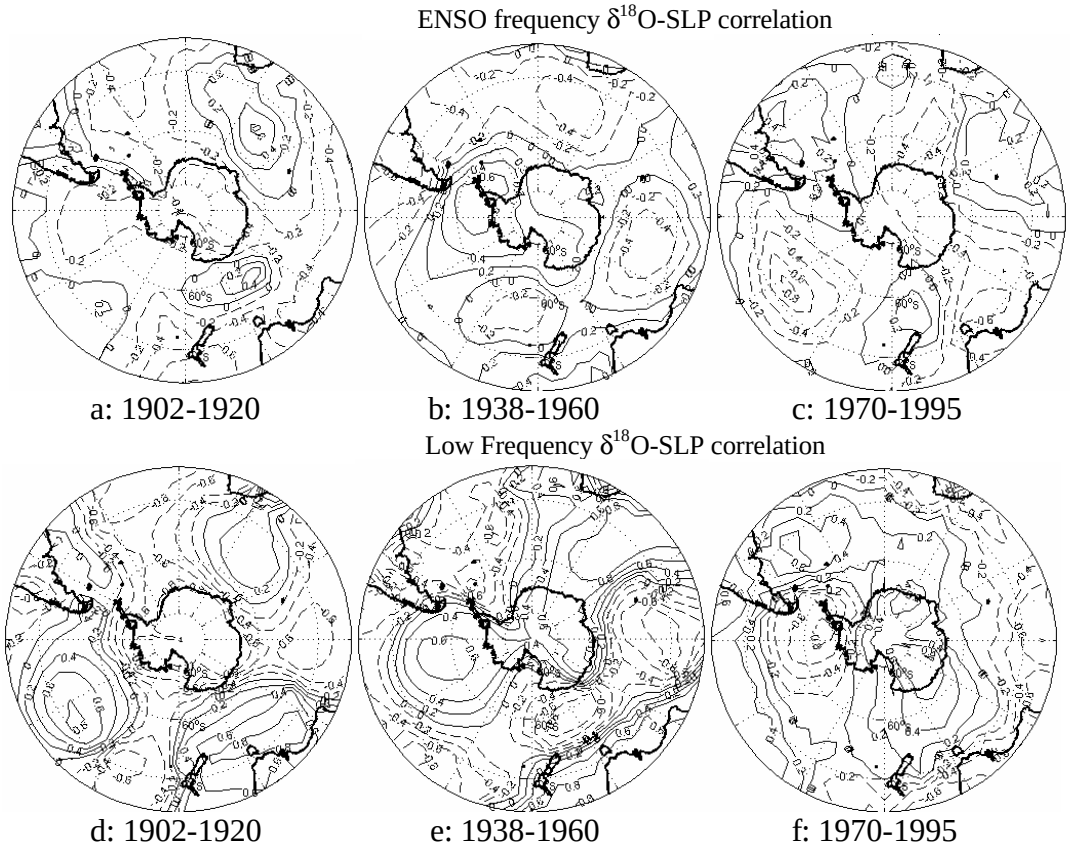

Figure 1: d^{18}O Correlated with SLP for three 20th century epochs of high ENSO activity. (a-c) Band Pass Filtered for ENSO frequency band of 3-6 year periods. (d-f) Low Pass filtered for periods longer than 6 years.

Turner 2004- Review- The El Niño Southern Oscillation and Antarctica, International Journal of Climatology 24, 1-31.

Steig, et al 2005: High-resolution ice cores from US-ITASE (West Antarctica): development and validation of chronologies and determination of precision and accuracy, Annals of Glaciology, 41, 77-84.

Zhang, Wallace, Battisti 1997: ENSO-like Interdecadal Variability: 1900–93, *Journal of climate 10,* 1004-1020.

Fogt and Bromwich 2006: Decadal Variability of the ENSO Teleconnection to the High-Latitude South Pacific Governed by Coupling with the Southern Annular Mode, *Journal of climate 19,* 979-997.

Thompson DWJ, Solomon S: Interpretation of recent Southern Hemisphere climate change: SCIENCE 296 (5569): 895-899 May 3 2002

The mean yearly temperature lapse rates in the urban atmospheric boundary layer (ABL) on microwave sounding data.

Kuznetsova I.N.[1], Khaikine M.N. [2], Nakhayev M.I. [1]
(muza@mecom.ru and khaikine@attex.ru)
[1] Hydrometeorological Research Center, Moscow, Russia
[2] Central Aerological Observatory, Dolgoprudny, Russia

The mean yearly temperature lapse rates were calculated using the data of ABL temperature profile measurements made by means of microwave meteorological temperature profiler MTP-5, developed in the Central Aerological Observatory /Kadygrov and Pick, 1998/. The measurements were carried out in three great cities of Russia: Moscow, Krasnoyarsk and Nijni Novgorod during 2004-2005 (table 1). These cities are located on approximately the same latitude but have different relief and landscape.

The lapse rate $G_h(t_i)$ were calculated using hourly averaged temperature $T_h(t_i)$ in the layers H=0-100, 0-200, 0-300, 0-400, 0-500 и 0-600 m. $G_h(t_i) = (T_0(t_i) - T_h(t_i))$ 100/h, where i=0,1,2... 23 is the number of the hour; t_i = 0:30; 1:30; 2:30... 23:30. $T_h(t_i)$ is mean temperature in i-th hour on height h; h=100, 200, 300, 400, 500 и 600 m.

Mean lapse rates calculated for the whole period of observations are given in Table 1. The minimum and maximum values of lapse rates and the value of mean square root deviations (MSRD) of daily mean lapse rates calculated for the layers is also shown in the table.

The temperature profile measurements were carried out in Moscow by MTP-5 placed in the center of the city. Table 1 shows the mean values of lapse rate vary in range from 0.42°C/100 m up to 1.77°C/100 m. It was noted that the ratio of maximum lapse rate to minimum one equals to almost constant value in all layers (it varies from 2.2 up to 2.5). The greatest variation of lapse rate observed in the lower 100 m layer. The mean lapse rate exceeds dry adiabatic gradient in the lower 100 m layer during 15 hours (from 8 up to 22 LT). The lower 300 m layer remains thermally unstable almost 12 hours (from 10 up to 21) and the whole 600-meter layer was unstable from 14 up to 16 (the instability maximum). Thus, the urban ABL is weakly-steady only third part of day. The conditions of intensive mixing and turbulent exchange are favorable for pollutions scattering observed in the largest part of day.

Profiler MTP-5 is installed in Krasnoyarsk in the center of city at a distance about 800 m from the Yenisey River. The lapse rate range of the intradiurnal changes (Max-Min difference in the day) was 1.8 times greater than that in the center of Moscow and MSRD was 1.6 times greater in Krasnojarsk than in Moscow in the lower 100 m layer. The lapse rates equaled to dry adiabatic gradients and greater were formed in Krasnoyarsk in the lower 300 m layer only in contrast to Moscow. It was observed in the layer 0-300 m for 3 hours (from 13 up to 16) and in the layer 0-100 m for 9 hours (from 10 up to 18), which is less for 7 hours than in Moscow (from 7 up to 22). The strong stability of ABL was observed in the lower 500 m layer from second half of the night (2-3 h) until the morning (7-8 h). Moreover, the layer 200-300 m was steadier than lower layer. It indicates existence of heat source, which decrease the cooling by radiation emission. Such source can be not only UHI, but also the water surface of Yenisey River. The influence of aqueous objects on the thermal regime of ABL is beyond controversy, but we do not have available quantitative estimations of such effects in the scale of a large city. Nevertheless, some conclusions can be done through comparison between consistent data from the three cities.

Nijni Novgorod is located on the banks of two large rivers: Volga River and Oka River. Profiler MTP-5 is installed in Nijni Novgorod on the high bank of Oka River at a distance about 900 m from the river. The maximum value of mean lapse rate in Nijni Novgorod was found to be 0.9°C/100 m, which is less than dry adiabatic gradient. This is the most essential difference from Moscow and Krasnoyarsk. An increase of the mean lapse rate with an increase of the layer thickness indicates the specific temperature conditions of ABL in Nijni Novgorod in the night and morning time (from 21 up to approximately 7) (in Moscow the picture is opposite). It is possible to assume that the moisture evaporating from the water table of two large rivers is the source of latent heat in the lower layers. Local winds formed due to a large difference of altitudes in coastal zone (greater than 100 m) can be

the reason for ABL structure deformations, but we do not have the data on the vertical stratification of wind and humidity to carry out the certain conclusions.

Conclusions

- greatest deformations of ABL thermal structure was observed in Moscow. It is caused by the multifactor influence of megalopolis on the thermal regime of the lower layers of the atmosphere;
- Yenisey River do substantial influence on urban ABL in Krasnoyarsk besides the city;
- ABL in Nijni Novgorod does not have expressed features of large city influence. The discovered specific features are probably caused by the influence of large river mirror and by local air circulations above the sharply heterogeneous relief.

The work was performed with the partial support by Russian Fund for Basis Research grants 05-05-65288-a, 06-05-644427 and 06-05-64104.

Table 1.

The mean yearly values of lapse rates (°C/100 m).

Hour	Moscow						Krasnojarsk						Nijni Novgorod					
	Layer, m																	
	100	*200*	*300*	*400*	*500*	*600*	*100*	*200*	*300*	*400*	*500*	*600*	*100*	*200*	*300*	*400*	*500*	*600*
0	**0,89**	**0,83**	**0,76**	**0,69**	**0,64**	**0,62**	0,21	0,15	0,16	0,16	0,19	0,24	0,06	0,13	0,20	0,23	0,27	0,32
1	**0,85**	**0,77**	**0,70**	**0,63**	0,59	0,57	0,11	0,06	0,07	0,09	0,13	0,18	0,01	0,07	0,14	0,18	0,23	0,28
2	**0,85**	**0,73**	**0,65**	0,58	0,55	0,53	0,05	***-0,01***	0,01	0,03	0,07	0,13	***-0,06***	0,01	0,09	0,14	0,20	0,25
3	**0,83**	**0,70**	**0,61**	0,54	0,51	0,49	***-0,02***	***-0,09***	***-0,06***	***-0,03***	0,02	0,08	***-0,12***	***-0,04***	0,04	0,10	0,16	0,22
4	**0,80**	**0,64**	0,56	0,49	0,46	0,45	***-0,06***	***-0,13***	***-0,11***	***-0,07***	***-0,02***	0,04	***-0,14***	***-0,06***	0,02	0,08	0,14	0,21
5	**0,80**	**0,62**	0,53	0,47	0,43	0,43	***-0,09***	***-0,17***	***-0,15***	***-0,11***	***-0,05***	0,01	***-0,14***	***-0,08***	0,00	0,07	0,13	0,19
6	**0,85**	**0,64**	0,53	0,46	0,43	0,42	***-0,06***	***-0,17***	***-0,16***	***-0,12***	***-0,07***	0,00	***-0,15***	***-0,11***	***-0,03***	0,03	0,09	0,16
7	**0,99**	**0,73**	**0,60**	0,51	0,46	0,45	0,09	***-0,08***	***-0,10***	***-0,08***	***-0,04***	0,02	***-0,05***	***-0,05***	0,00	0,05	0,11	0,17
8	**1,20**	**0,90**	**0,73**	**0,62**	0,56	0,53	0,36	0,12	0,05	0,03	0,05	0,10	0,14	0,06	0,08	0,11	0,15	0,20
9	**1,42**	**1,09**	**0,92**	**0,78**	**0,69**	**0,65**	**0,71**	0,37	0,25	0,19	0,18	0,21	0,38	0,26	0,23	0,23	0,25	0,29
10	**1,57**	**1,27**	**1,07**	**0,91**	**0,81**	**0,75**	**1,01**	**0,61**	0,45	0,36	0,33	0,33	0,58	0,44	0,39	0,36	0,36	0,39
11	**1,67**	**1,38**	**1,18**	**1,02**	**0,91**	**0,85**	**1,30**	**0,87**	**0,68**	0,55	0,49	**0,49**	**0,73**	0,58	0,52	0,47	0,46	0,48
12	**1,74**	**1,46**	**1,27**	**1,10**	**0,98**	**0,92**	**1,51**	**1,07**	**0,86**	**0,71**	**0,63**	**0,61**	**0,84**	**0,69**	**0,62**	0,57	0,55	0,55
13	**1,76**	**1,50**	**1,32**	**1,14**	**1,03**	**0,97**	**1,62**	**1,20**	**0,99**	**0,82**	**0,74**	**0,70**	**0,89**	**0,76**	**0,69**	**0,63**	**0,61**	**0,61**
14	**1,77**	**1,52**	**1,34**	**1,17**	**1,05**	**0,99**	**1,62**	**1,23**	**1,03**	**0,87**	**0,78**	**0,75**	**0,90**	**0,79**	**0,72**	**0,67**	**0,64**	**0,64**
15	**1,75**	**1,51**	**1,34**	**1,17**	**1,06**	**1,00**	**1,55**	**1,20**	**1,03**	**0,87**	**0,79**	**0,76**	**0,87**	**0,77**	**0,72**	**0,67**	**0,65**	**0,65**
16	**1,71**	**1,49**	**1,33**	**1,16**	**1,05**	**0,99**	**1,42**	**1,14**	**0,99**	**0,85**	**0,78**	**0,75**	**0,80**	**0,73**	**0,69**	**0,65**	**0,63**	**0,64**
17	**1,63**	**1,44**	**1,29**	**1,14**	**1,03**	**0,97**	**1,26**	**1,04**	**0,92**	**0,79**	**0,73**	**0,71**	**0,72**	**0,67**	**0,64**	**0,61**	**0,60**	**0,61**
18	**1,55**	**1,37**	**1,23**	**1,09**	**0,99**	**0,94**	**1,11**	**0,94**	**0,84**	**0,73**	**0,68**	**0,67**	**0,63**	0,59	0,59	0,56	0,56	0,58
19	**1,40**	**1,27**	**1,16**	**1,03**	**0,94**	**0,89**	**0,95**	**0,83**	**0,76**	**0,67**	**0,63**	**0,62**	0,55	0,53	0,53	0,52	0,52	0,54
20	**1,23**	**1,15**	**1,06**	**0,95**	**0,88**	**0,84**	**0,79**	**0,70**	**0,65**	0,58	0,55	0,55	0,48	0,47	0,48	0,47	0,48	0,50
21	**1,07**	**1,04**	**0,97**	**0,88**	**0,81**	**0,78**	**0,60**	0,55	0,52	0,47	0,46	0,48	0,34	0,37	0,40	0,41	0,43	0,46
22	**0,99**	**0,96**	**0,89**	**0,80**	**0,75**	**0,72**	0,44	0,40	0,40	0,37	0,37	0,40	0,25	0,28	0,32	0,35	0,38	0,41
23	**0,95**	**0,89**	**0,83**	**0,75**	**0,70**	**0,67**	0,31	0,27	0,27	0,26	0,28	0,31	0,15	0,20	0,26	0,29	0,33	0,38
Min	**0.80**	**0.62**	**0.53**	**0.46**	**0.43**	**0.42**	**-0.09**	**-0.17**	**-0.16**	**-0.12**	**-0.07**	**.00**	**-0.15**	**-0.11**	**-0.03**	**0.03**	**0.09**	**0.16**
Max	**1.77**	**1.52**	**1.34**	**1.17**	**1.06**	**1.00**	**1.62**	**1.23**	**1.03**	**0.87**	**0.79**	**0.76**	**0.90**	**0.79**	**0.72**	**0.67**	**0.65**	**0.65**
MSRD	**0.38**	**0.33**	**0.30**	**0.26**	**0.23**	**0.21**	**0.61**	**0.50**	**0.43**	**0.36**	**0.31**	**0.27**	**0.38**	**0.32**	**0.27**	**0.22**	**0.19**	**0.17**

Reference.

Kadygrov E.N., Pick D.R. 1998. The potential for temperature retrieval from an angular- scanning single-channel microwave radiometer and some comparisons with in situ observations. //Meteorological Application, UK, p. 393-404

Cross-wavelet analysis of coherence and time lags between El Niño and Atlantic equatorial mode

I.I. Mokhov[1], V.A. Bezverkhny[1], A.A. Karpenko[1], N.S. Keenlyside[2] and S.S. Kozlenko[1,3]

[1]A.M. Obukhov Institute of Atmospheric Physics RAS, Moscow, Russia
[2] Leibniz-Institut für Meereswissenschaften, Kiel, Germany
[3] Moscow Institute for Physics and Technology, Dolgoprudny, Russia
mokhov@ifaran.ru

An observational-based analysis of time lags between equatorial Pacific mode (El Niño–Southern Oscillation or ENSO) and equatorial Atlantic mode (EAM) is performed. EAM (Zebiak, 1993) is similar to ENSO (see (Keenlyside and Latif, 2007)).

We used several monthly mean indices for El Niño (EN) and EAM based on the HADISST data set (Rayner et al., 2003) for sea surface temperature (SST) since January 1870 till May 2006: Niño3 (5S-5N, 150W-90W) and Niño3.4 (5N-5S, 170W-120W) in the Pacific and Atlantic3 (20W-0, 3S-3N) in the Atlantic (see also (Keenlyside and Latif, 2007)).

Interaction between EN and EAM was studied with the use of different cross-wavelet analyses (CWA) of time series for SSTs and SST anomalies (SSTAs): CWA-1 (Bezverkhny, 2001; Mokhov et al., 2005) and CWA-2 (Jevrejeva et al., 2003; Grinsted et al., 2004).

The CWA results display differences in the local coherence and phase lags between SSTAs in regions Niño3/Niño3, 4 and Atlantic3 for different periods during 1870-2006. Figure 1 shows local coherence between SSTAs for Niño3 and Atlantic3 obtained with the use CWA-1. According to Fig.1, positive values of coherence dominate for short-term cycles (with periods about 1-2 years). At the same time, for a significant part of the total analyzed interval 1870-2006, regimes with the El Niño lagging the EAM are displayed. For cycles with large periods (from about 3-5 years) there are time intervals with positive and negative coherence and phase lags.

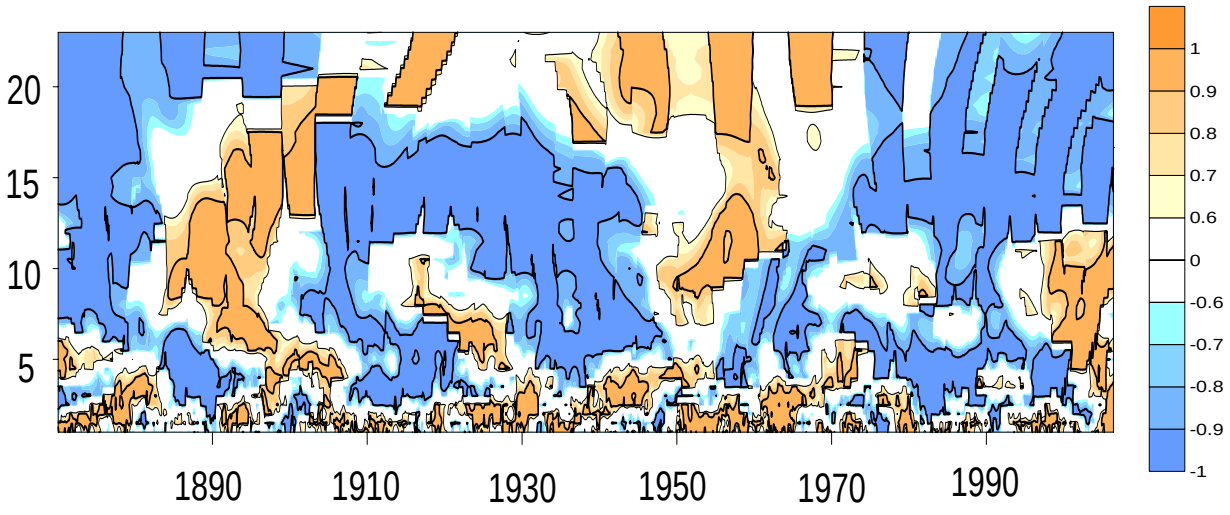

Figure 1. Local coherence between SSTAs for Niño3 and Atlantic3.

It will be interesting to compare these results with results of corresponding analysis with the use of methods based on phase dynamics modeling and nonlinear "Granger causality" applied by Mokhov and Smirnov (2006a,b) to the analysis of mutual dynamics of ENSO and North Atlantic Oscillation.

This work was partly supported by the Russian Foundation for Basic Research, Programs of the Russian Academy of Sciences, Russian President Scientific Grant and NATO Collaborative Linkage Grant.

References

Bezverkhny, V.A., 2001: Developing the wavelet-transform method for analysis of geophysical data. *Izvestiya, Atmos. Oceanic. Phys.*, **37** (5), 584-591.

Grinsted, A., J.C. Moore, and S. Jevrejeva, 2004: Application of the cross wavelet transform and wavelet coherence to geophysical time series. *Nonlin. Proc. Geophys.*, **11**, 561-566.

Jevrejeva, S., J.Moore, A. Grinsted, 2003: Influence of the Arctic Oscillation and El Nino – Southern Oscillation (ENSO) on ice conditions in the Baltic Sea: The wavelet approach. *J. Geophys. Res.*, **108** (D21), 4677, doi:10.1029/2003JD003417.

Keenlyside, N.S., and M. Latif, 2007: Understanding Equatorial Atlantic Interannual Variability. *J. Climate*, **20**, 131-142.

Mokhov, I.I., V.A. Bezverkhny, A.A. Karpenko, 2005: Diagnosis of relative variations in atmospheric greenhouse gas contents and temperature from Vostok Antarctic ice core paleoreconstructions. *Izvestiya, Atmos. Oceanic. Phys.*, **41** (5), 523-536.

Mokhov, I.I., and D.A. Smirnov, 2006a: El Niño–Southern Oscillation drives North Atlantic Oscillation as revealed with nonlinear technique from climatic indices. *Geophys. Res. Lett.*, **33**, L03708, doi:10.1029/2005GL024557.

Mokhov, I.I., and D.A. Smirnov, 2006b: Study of the mutual influence of the El Nino – Southern Oscillation processes and the North Atlantic and Arctic Oscillations. *Izvestiya, Atmos. Oceanic. Phys.*, **42** (5), 598-614.

Rayner, N.A, D. E. Parker, E. B. Horton, C. K. Folland, L. V. Alexander, D. P. Rowell, E. C. Kent and A. Kaplan, 2003: Global analyses of sea surface temperature, sea ice, and night marine air temperature since the late nineteenth century. *J. Geophys. Res.*, **108** (D14), doi:10.1029/2002JD002670.

Zebiak, S.E., 1993: Air-sea interaction in the equatorial Atlantic region. *J. Climate*, **6**, 1567-1586.

Circulation indices extremes in seasonal hindcast integrations

A.V.Muraviev, I.A. Kulikova, and E.N.Kruglova
Hydrometeorological Research Centre of the Russian Federation
Bol. Predtechensky per., 11-13, 123242 Moscow, Russia
e-mail: muravev@mecom.ru

Large scale circulation patterns may be described by characteristics, similar to the five well-known "pattern indices" (*Wallace, and Gutzler*, 1981), but calculated for daily rather then for monthly geopotential 500 mb height fields. Here the atmosphere is assumed to pass through different "weather" or "flow" regimes resulting from nonlinear synoptic-planetary scales interaction (*Reinhold, and Pierrhumbert*, 1982). These regimes are defined and assessed by extreme values of correspondent circulation indices (CI) thus reducing the problem to the analysis of outliers and extremes in daily quantized modeled and observed time series.

The global spectral T41L15 GCM has been integrated in a hindcast mode out to 90 days with initial data obtained from the NCEP/NCAR reanalysis archive starting from 31.06 and 30.11 every year during 1983-2002. This model is operationally used for monthly and seasonal hydrodynamic-statistical ensemble forecasts at the Russian HMC (*Muraviev et al, 2005*).

The scatter diagrams for the first 10 days show the correlation between modeled and observed index values (e.g. Fig.1). Let us label the correlation coefficients (CC) with the Wallace-Gutzler pattern notation. The CCs for all five circulation indices, depicting the GCM utility at medium-ranges, descend as follows:
summer CC_{PNA}=0.74; winter CC_{PNA}=0.70; summer CC_{WA}=0.69; winter CC_{WP}=0.68; winter CC_{EA} =0.65;
summer CC_{EU} =0.64; winter CC_{EU}= 0.63; summer CC_{EA} =0.53; winter CC_{WA}=0.47; summer CC_{WP}=0.39.

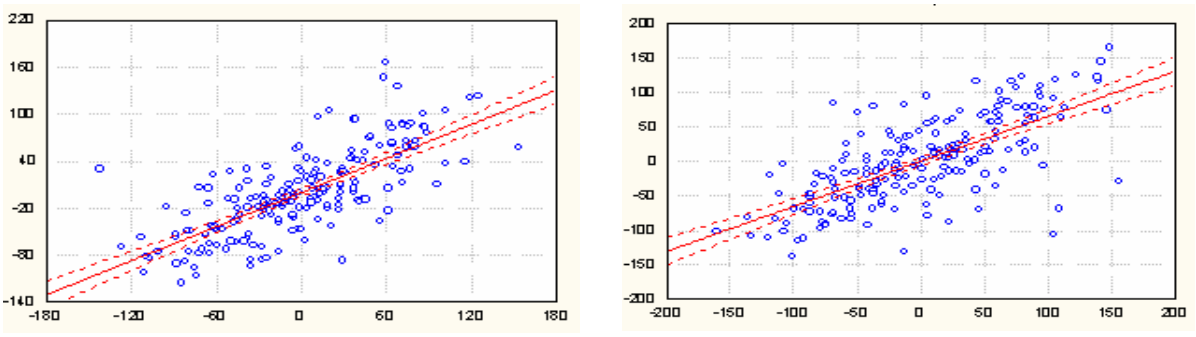

(a) (b)

Fig.1. Scatter diagrams for PNA index in first 10 days summer (a) and winter (b) integrations. Dotted lines indicate 95%-confidence for regression. Index values are multiplied by 100.

The variation of the correlation at medium ranges yields the PNA index as the most predictable, and the "seesaws" WA and WP in western ocean regions – as the least predictable, what quite good corresponds to the skill of the GCM in forecasting some other fields. The quantile-quantile plots of the full sample of 1800 values (90 days × 20 years) represent the outlier deviation from the normal distribution (Fig.2).

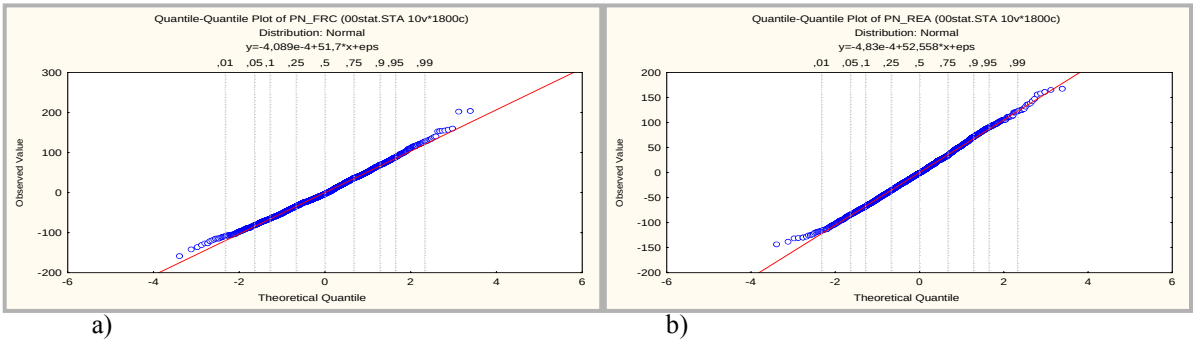

a) b)

Fig.2. Quantile plots against normal distribution for the winter PNA index. Left side (a) shows forecast data, right side (b) shows reanalysis data. Tail regions along the line indicate deviation of extremes from normal distribution. Index values are multiplied by 100.

In consideration of sampling errors a set of thresholds has been used for "box and whisker" plots (Fig.3). The quartiles L(25%) and H(75%) are used for calculating the span $\Delta = H - L$. Thresholds $\alpha(i)$, i=1 ...n , define *outliers* as index values being outside of $[L - \alpha(i)\cdot\Delta,\ H + \alpha(i)\cdot\Delta]$, and *extremes* as values being outside of $[L - 2\cdot\alpha(i)\cdot\Delta,\ H + 2\cdot\alpha(i)\cdot\Delta]$.

a) b)

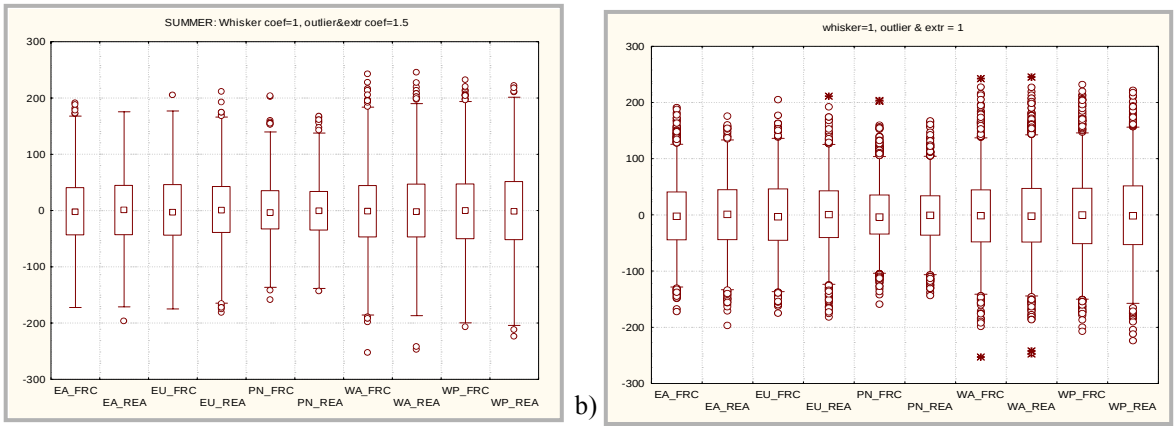

Fig.3. Box and whiskers for summer CIs: left side (a) shows *outliers* for α=1.5, right side (b) shows *outliers* and *extremes* for α=1.0. The box-whiskers correspond to EA, EU, PNA, WA, and WP indices with 'FRC' denoting forecast, and 'REA' denoting reanalysis. Boxes stand for $\Delta = H - L$, whiskers stand for 'non-outlier' interval, circles denote *outliers*, asterisks denote *extremes*.

A usual statistical approach in defining extremes is evidently crude in defining meteorologically 'large anomalies'. Fig.3 is to certify that thresholds near recommended α=1.5 exclude events which we would like to call *extremes* with statistical property. In particular the right side of Fig.3 yields several informal conclusions. For instance, the largest number of WA index extremes of both signs indicate the atmospheric *instability* and *variability*, which are more *predictable* in the extreme-statistical sense, than the EA or PNA indices.

Collected diagram data are used for extremes' statistics, their *recurrence* and *duration* (see Table). These statistics may be applied both to concomitant synoptic events and to the GCM skill in predicting these features at seasonal time scales. Comparing medium and seasonal ranges one may note, that the PNA and EU indices predictability may be considered as opposed (see Fig.1 and EU, PNA columns in Table).

Table.
Recurrence and duration for several summed CIs outliers and extremes in winter seasons 1983-2002. Columns denote upper and lower CI values (×100) for two α thresholds (from top +1.5, +1.0, -1.0, -1.5), days number with CI extremes (2), minimum (3) and maximum (4) duration in days, and mean duration (5) in days.

1	2	3	4	5
EU_FORECAST				
193	0	0	0	0
145	20	1	4	1.8
-145	15	1	5	1.7
-193	0	0	0	0
EU_REANALYSIS				
187	2	2	2	2
140	23	1	5	1.6
-140	21	1	5	1.4
-187	2	1	1	1

1	2	3	4	5
PNA_FORECAST				
161	5	1	1	1
121	37	1	4	1.8
-121	22	1	5	1.8
-160	3	1	1	1
PNA_REANALYSIS				
200	0	0	0	0
150	5	1	1	1
-150	19	1	3	1.5
-200	1	1	1	1

1	2	3	4	5
WP_FORECAST				
194	11	1	4	2.2
145	40	1	8	2
-151	22	1	5	1.7
-200	4	1	2	1.3
WP_REANALYSIS				
214	9	1	3	1.8
160	57	1	6	2
-164	19	1	4	1.9
-218	1	1	1	1

1. Wallace J.M., and D.S. Gutzler, 1981: Teleconnections in the geopotential height field during the Northern Hemisphere winter. *Monthly Weather Review*, **109**, 784-812.
2. Reinhold B.B., and R.T. Pierrehumbert, 1982: Dynamics of weather regimes: quasi-stationary waves and blocking. *Monthly Weather Review*, **110**, 1105-1145.
3. Muraviev A.V., I.A. Kulikova, E.N. Kruglova, V.D. Kaznacheeva, 2005: Using ensembles in hydrodynamic-statistical meteorological forecasting. *Russian Meteorology and Hydrology*, **7**, 3 – 15.

Southern Sea Ice, cyclone behaviour and rainfall in Melbourne and Perth

Alexandre Bernardes Pezza, Tom Durrant, Ian Simmonds and Ian Smith
School of Earth Sciences, The University of Melbourne, Victoria 3010, Australia
e-mail: apezza@unimelb.edu.au

We explore the relationship between Southern Hemisphere (SH) sea ice extent (SIE) given in pre-defined sectors around Antarctica and rainfall in Perth and Melbourne, respectively located in the south-western and south-eastern corners of Australia. Significant decreasing trends in rainfall in the seventies particularly over Perth followed by a more recent strong negative tendency in both regions have motivated this study after it has been identified that SIE significantly interacts with the general circulation (Kwok and Comiso, 2002). The principal aim is to determine if the rainfall time series relate to any of the five main ice sectors around Antarctica (figure 1) via changes in cyclone and anticyclone behaviour. The study covers the 'satellite era' from 1979 to 2003, and results are presented for the wintertime (JJA) when midlatitude baroclinicity is enhanced.

Results suggest that high (low) sea ice extent is associated with low (high) rainfall in both localities, more significantly in Perth (figure 2). Local and upstream sectors of the ice appear most associated, i.e., the Indian Ocean sector with Perth rainfall, and the West Pacific sector south of Australia with Melbourne rainfall. An automatic tracking scheme applied to the National Centers for Environmental Prediction (NCEP) reanalysis-2 data suggests a possible link between SIE and the winter storms affecting Perth and Melbourne via a well defined anomalous pattern impinging from midlatitudes which resembles some of the recent links found between the circulation and the Pacific Decadal Oscillation (PDO, Pezza et al 2007).

The possible impacts of a third party mechanism influencing both the ice and the circulation leading to rainfall anomalies are discussed in terms of the El Niño/Southern Oscillation (ENSO) and the Southern Annular Mode (SAM), which are known to modulate rainfall anomalies in Australia. The results suggest that when the ENSO influences are isolated the same relationship between SIE and rainfall is still observed, however this is not true for the SAM. Here we propose SAM and SIE as being part of a complex coupled mechanism which is relatively independent from ENSO. These associations add insight to the recent literature and may help to understand the large scale mechanisms potentially associated to declining trends in

Australian rainfall. Further results are under investigation and will be published in the peer-reviewed literature in the near future.

Kwok, R., and Comiso, J.C., 2002: Southern Ocean climate and sea ice anomalies associated with the Southern Oscillation. *Journal of Climate*, **15**, 487-501.

Pezza, A.B., Simmonds, I. and Renwick, J, 2006: Southern Hemisphere cyclones and anticyclones: Recent trends and links with decadal variability in the Pacific Ocean. *International Journal of Climatology*, in press.

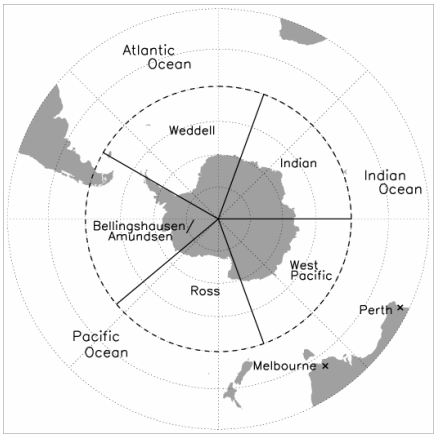

Figure 1: Polar Stereographic plot showing the five sectors used to calculate the sea ice extent. The locations of Perth and Melbourne are also indicated.

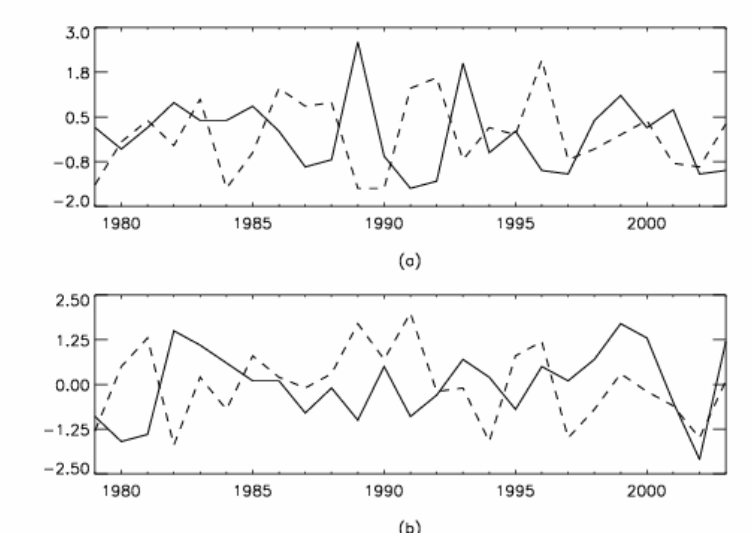

Figure 2: (a) Perth rainfall and Indian Ocean SIE and (b) Melbourne rainfall and West Pacific SIE anomalies for JJA 1973 – 2003. Rainfall is given by dashed lines and SIE is given by solid lines.

The climatic importance of South Atlantic hurricane Catarina (2004)

Alexandre Bernardes Pezza and Ian Simmonds
School of Earth Sciences, The University of Melbourne, Victoria 3010, Australia
e-mail: apezza@unimelb.edu.au

Sea Surface Temperatures (SSTs) warmer than 26.5^{o}C and Environmental Vertical Wind Shear (EVWS) lower than 8 m/s offer ideal conditions for Tropical Cyclone (TC) development. Thus it has been accepted that hurricanes could not form over the South Atlantic Ocean due to the very intense climatological EVWS and not sufficiently warm SSTs over the basin. This concept is now under review after Catarina hit southern Brazil in March 2004 (figure 1) after undergoing Tropical Transition (TT) over relatively cool waters (figure 2). This was the first documented time when a system reaching a category I hurricane strength (Saffire-Simpson scale) made landfall anywhere in the South Atlantic basin (Pezza and Simmonds 2005). This is not to say that a phenomenon like Catarina had not existed in the past, but there is evidence that at least during the satellite era this is unprecedented.

Catarina generated much discussion and controversy in the community as to how it should be named (which also depends on cultural backgrounds) and as to what its hybrid structure really was. This hurricane represents a mark in Southern Hemisphere meteorology prompting the weather services to improve their forecasting and alert system in a time of climate change. It also draws the attention of the global meteorological community for the increasing need to develop a more modern system of classification of cyclones.

Pezza and Simmonds (2005) proposed a large scale blocking mechanism leading to persistent low EVWS to explain how this extremely rare event was formed, and such ideas have recently received further support in the literature (McTaggart-Cowan et al 2006). A possible hemispheric link with the positive phase of the Southern Annular Mode (SAM) has been found, pointing out to the possibility of more frequent storms if the SAM continues to increase under global warming conditions. We are currently working on further evidence for this association and the new results will be communicated in the peer-reviewed literature. Advances in modeling and the local observing network are expected to throw further light into a possible hurricane climate prediction scheme for the region in the future.

McTaggart-Cowan, R., Bosart, L., Davis, C.A., Atallah, E.H., Gyakum, J.R. and Emanuel, K., 2006: Analysis of hurricane Catarina (2004). *Monthly Weather Review*, **134**, 3029-3053.

Pezza, A.B., and Simmonds, I, 2005: The first South Atlantic hurricane: Unprecedented blocking, low shear and climate change. *Geophysical Res. Letters,* **32**, doi:10.1029/2005GL023390.

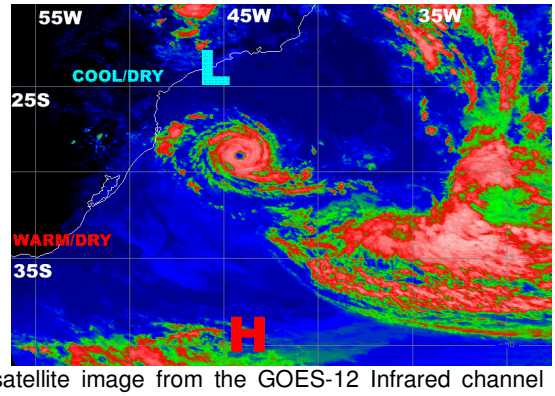

Figure 1: Enhanced satellite image from the GOES-12 Infrared channel at 16:39 UTC 26th March 2004 showing the Tropical Cyclone Catarina approaching the Brazilian coast. The letters H and L indicate the position of the upper level ridge and trough respectively associated with warm/dry and cool/dry surface air over the continent. Estimated minimum central pressure inside the eye of 974 hPa, total cyclone diameter of around 400 Km and eye diameter between 25 and 40 Km, with estimated sustained surface winds with hurricane I force (between 33 m/s and 42 m/s) and translational speed of 11 km/h to the west. Image available for download from the University of Wisconsin – Madison Space Science and Engineering Center (http://cimss.ssec.wisc.edu)

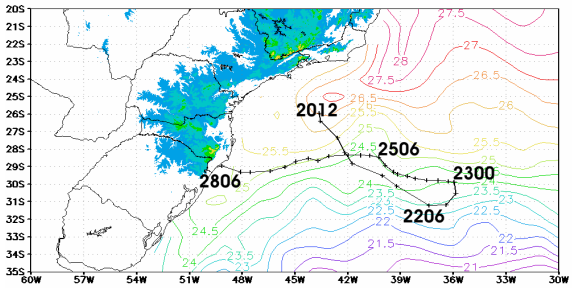

Figure 2: Tropical Cyclone Catarina's trajectory in perspective with the surrounding maximum Sea Surface Temperatures (SSTs). The South American sector is showing: I) 2 km resolution topography plotted for elevations above 500 m, with darker yellow tones indicating elevations above 1500 m; II) Tropical cyclone Catarina's trajectory as derived from the University of Melbourne automatic tracking algorithm showing the central locations every 06 hours and III) Maximum SSTs (°C) for the period between the 20th and the 28th of March. The date and hour (UTC) are indicated next to the trajectory for some selected periods.

A ferocious and extreme Arctic storm in a time of decreasing sea ice

Ian Simmonds* and Mark R. Drinkwater**

*School of Earth Sciences
The University of Melbourne
Victoria, 3010, Australia
simmonds@unimelb.edu.au

**European Space Agency
Earth Observation Programmes
Postbus 299, 2200 AG Noordwijk
The Netherlands
Mark.Drinkwater@esa.int

Summer Arctic sea-ice extent has exhibited a downward trend since comprehensive satellite data became available in 1979. The decline has been especially steep since 2002 (Stroeve et al. 2005) and a record low was set in September 2005. Ice extent from January through to the middle of July 2006 was well below 2005 conditions, and the August 2006 sea ice extent was only slightly greater than the 2005 record set for that month (NSIDC, http://www.nsidc.org).

Against this background, much public and media interest was attracted in connection with analyses of the remarkable Arctic ice conditions and severe storms in August 2006 (ESA, 2006). Data from ESA's Envisat's Advanced Synthetic Aperture Radar (ASAR) instrument showed that sea ice that had survived the melt season had been fragmented by fierce late summer storms, as a consequence of surface wind-forced ice drift divergence. We are exploring the complex relationships between Arctic cyclones and sea-ice distribution, a topic of particular concern during a period of dramatic sea-ice decrease.

We report here on a very powerful synoptic event which occurred in the central Arctic in August 2006. We have used MSLP fields from the NCEP/DOE reanalysis in conjunction with the Melbourne University cyclone tracking scheme (Murray and Simmonds 1995, Simmonds et al. 2003) to objectively locate and track all cyclones that occurred in the Arctic basin (70-90^{o}N) in the month August 2006. The cyclone of interest here was very intense and lasted a significant proportion of the month. Fig. 1 (left) shows the cyclone on 18 August 12UTC at which time it achieved its lowest central pressure of 983.8 hPa (which is within the second percentile of all August cyclones in the basin (1979-2006)). Even more dramatic was the system's Depth (17.2 hPa at 6UTC) and Laplacian (2.57 hPa (deg. lat.)$^{-2}$ at 19 August 0UTC). Both these values fall within the first half-percentile of their respective August climatological distributions (Fig. 2). This was indeed a ferocious and extreme event.

The Envisat satellite-derived ASAR image mosaics and daily tracked sea-ice drift reveal the response of sea-ice pack to this ferocious and extreme summer event (Fig. 1 (right)). Ice divergence results in significant reduction in sea-ice concentration, with the consequence of enhanced positive albedo feedback.

ESA, 2006: Arctic summer ice anomaly shocks scientists, Unpublished Web article http://www.esa.int/esaEO/SEM7ZF8LURE_index_0.html

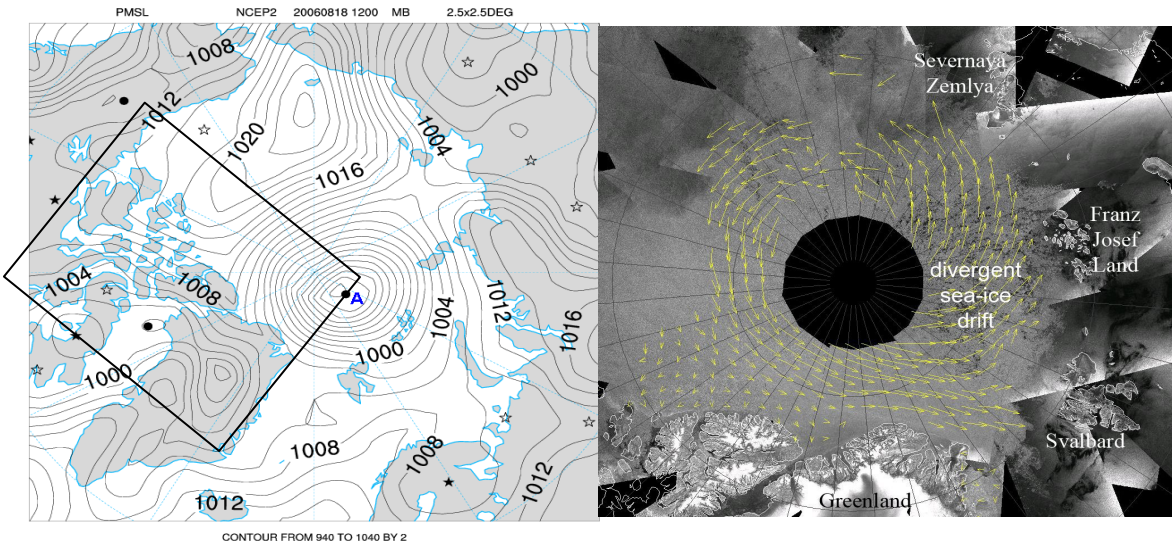

Fig. 1: (left) NCEP/DOE MSLP reanalysis at 18 August 2006 12UTC (contour interval 2 hPa). The intense cyclone of interest is marked with an 'A', and the box indicates the location of the satellite image mosaic in the right panel. Corresponding 30d mean daily ice drift vectors (right) for the month of August, superimposed on the 24 August Envisat ASAR Arctic image mosaic (courtesy Leif Toudal-Pedersen, PolarView consortium).

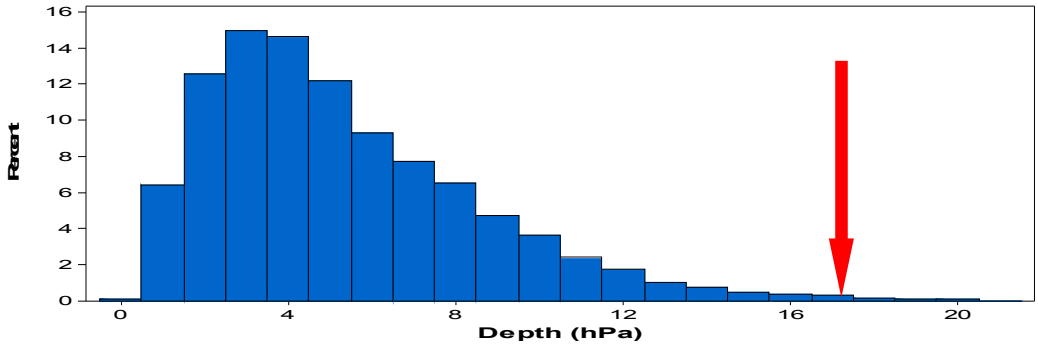

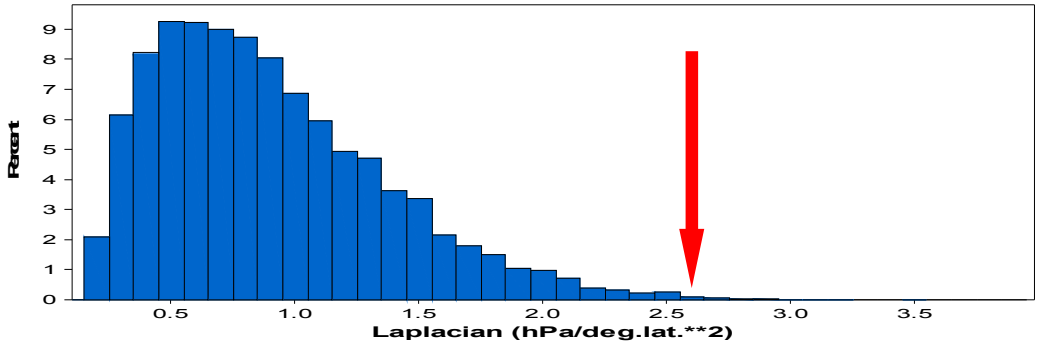

Fig. 2: Histograms of the distributions of (top) Depth and (bottom) Laplacian of MSLP of all August cyclones in the domain 70-90ºN (1979-2006). The red arrows indicate the values diagnosed for the 18/19 August 2006 event.

An analytical expression for the amplitude of wavenumber-one vertical velocity in the inner-core region of tropical cyclones under the influence of vertical ambient shear

Mitsuru Ueno
Typhoon Research Department, Meteorological Research Institute
e-mail: mueno@mri-jma.go.jp

It is well known that mature tropical cyclones exhibit highly axially symmetric structure in the core. On the other hand, recent observational studies (e.g., Corbosiero and Molinari 2002; Ueno 2005) have shown that convective activities tend to be enhanced on the down-shear to downshear-left side of the storm rather than evenly significant in the eyewall annulus. In the present study an analytical expression for the magnitude of wavenumber-one vertical motion asymmetries in the inner-core region of tropical cyclones under the influence of vertical ambient shear is derived in an attempt to understand the underlying mechanism for the initiation of asymmetric convection by vertical shear.

As illustrated by Jones (1995), in the situation that the vertical shear tends to tilt the vortex in the vertical, the vertical shear of the azimuthal flow tends to change in the opposite sense between the locations of maximum tangential wind and elsewhere since the vortex flow varies with radius such that the tangential wind speed increases from the center to a radius then decreases. Then consistency with thermal wind balance requires that a pair of temperature anomalies of opposite sign is generated with a positive (negative) anomaly on the upshear (downshear) side. This temperature perturbation should be achieved by vertical circulation. Based on these considerations, the vertical motion due to vertical wind shear may be quantified in the following manner.

The thermal wind balance equation for an axisymmetric typhoon-like vortex may be written in pressure coordinates as

$$\left(f + \frac{2v}{r} \right) \frac{\partial v}{\partial p} = -\frac{R}{p} \left(\frac{\partial T}{\partial r} \right)_p , \qquad (1)$$

where v is tangential wind speed, and remaining symbols are conventional. Now consider a situation in which every portion of an initially upright vortex is being horizontally advected by the environmental wind at each level. Then the vertical shear of the azimuthal flow (i.e., $\partial v / \partial p$) evaluated at p_M level and at a point on the downtilt side of the vortex center would change by $\partial v / \partial r \times S \delta t$ during the time period δt , where S is the vertical shear of the environmental wind evaluated at p_M . Letting the corresponding temperature change at the point δT and assuming that Eq. (1) holds even for the tilted vortex at least locally, we may obtain

$$\left(f + \frac{2v}{r} \right) \left(\frac{\partial v}{\partial r} \right)_p S \delta t = -\frac{R}{p} \left(\frac{\partial \delta T}{\partial r} \right)_p .$$

Assuming that the temperature tendency is totally accounted for by the temperature change due to vertical motion within the framework of dry adiabatic dynamics, and solid-body rotation to characterize the winds inside the radius of maximum wind, we can finally arrive at the following

simple formula for the azimuthal wavenumber-one component of vertical velocity at the radius of maximum wind r_m ,

$$\omega_1 = -\frac{p}{R} v_m \left(f + \frac{2v_m}{r_m} \right) S \Big/ \left(\frac{\kappa T}{p} - \frac{\partial T}{\partial p} \right),$$

where v_m is the maximum tangential wind at p_M .

Next we attempt to validate the analytical solution obtained above by numerical model results. Figure 1 shows a time series of the magnitude of azimuthal wavenumber-one vertical motion, comparing the analytical solutions with the results from some dry model integrations. Details of the present study can be found in Ueno (2007).

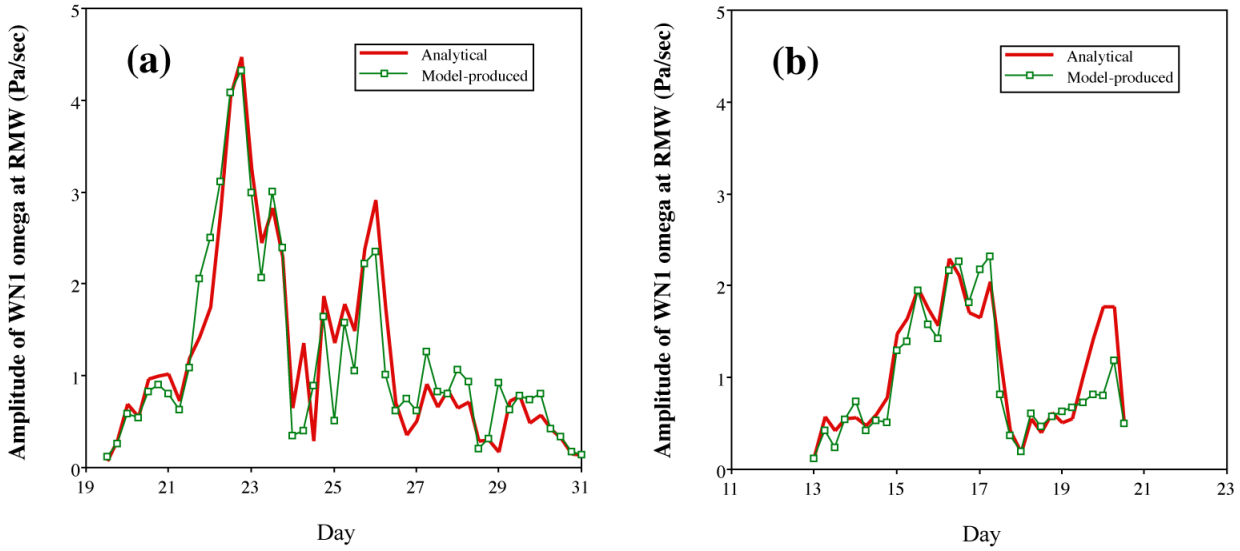

Figure 1: Comparison of "analytical" (thick red line) and model-simulated (thin green line with open squares) wavenumber-one omega (i.e., vertical p-velocity in units of Pa s^{-1}) at RMW and at 1 h of the consecutive 6-hourly dry integrations for (a) Typhoon Chaba and (b) Typhoon Tokage in 2004. The horizontal axis denotes the initial time of the integrations with numbers indicating day of the month, that is, August for (a) and October for (b), located at 00 UTC.

References

Corbosiero, K. L., and J. Molinari, 2002: The effects of vertical wind shear on the distribution of convection in tropical cyclones. ***Mon. Wea. Rev.***, **130**, 2110-2123.

Jones, S. C., 1995: The evolution of vortices in vertical shear. I: Initially barotropic vortices. ***Quart. J. Roy. Meteor. Soc.***, **121**, 821-851.

Ueno, M., 2005: Relationship between storm motion, vertical wind shear and rainfall asymmetries in typhoons. ***Kaiyo Monthly*** , **42** (Special Volume), 120-126 (in Japanese).

Ueno, M., 2007: Observational analysis and numerical evaluation of the effects of vertical wind shear on the rainfall asymmetry in the typhoon inner-core region. (***J. Meteor. Soc. Japan***, in press)